# SUSTAINABLE AND EFFICIENT ENGINEERING SOLUTIONS: MATERIALS DESIGN, MANUFACTURING AND AI

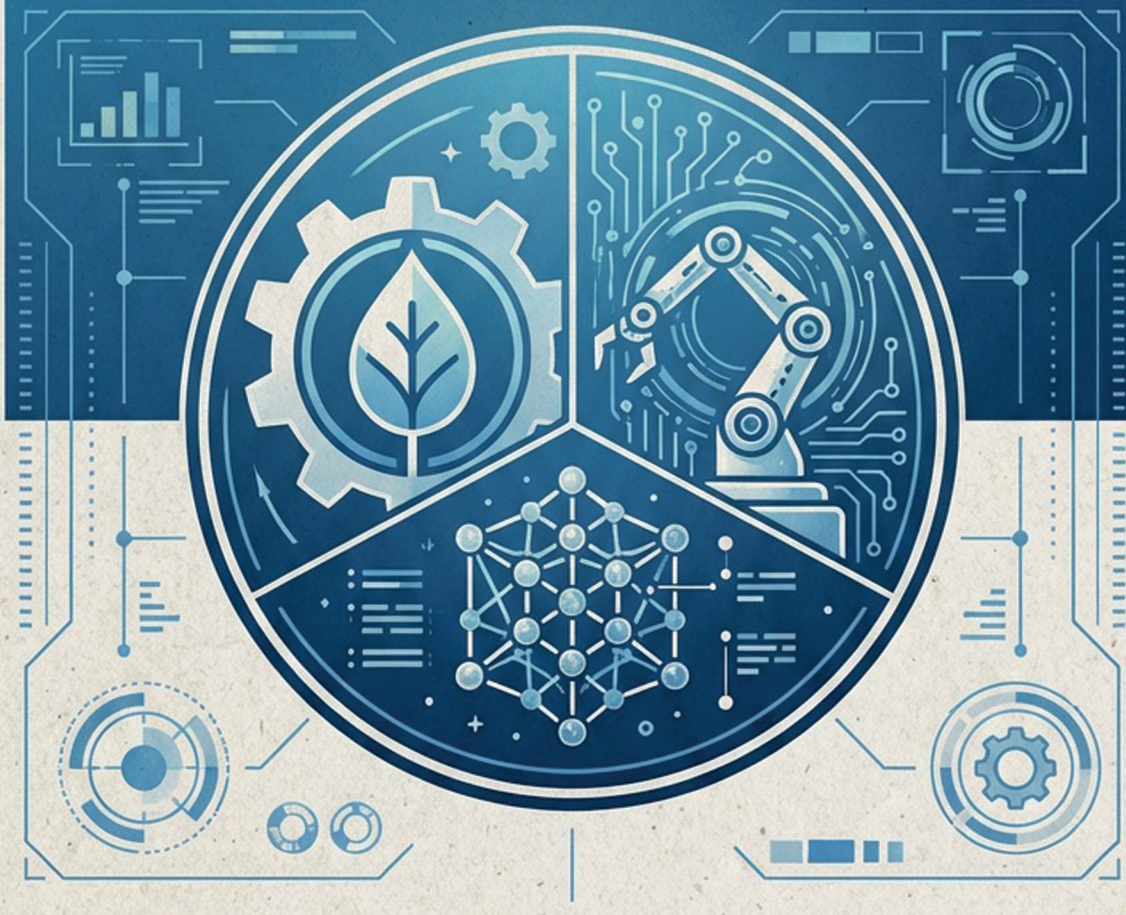

Editor: Assoc. Prof. Dr. Mehmet AKKAŞ

DUVAR

# SUSTAINABLE AND EFFICIENT ENGINEERING SOLUTIONS: MATERIALS DESIGN, MANUFACTURING AND AI

**Editor:Assoc. Prof. Dr. Mehmet AKKAŞ**

***Sustainable and Efficient Engineering Solutions: Materials Design, Manufacturing and AI***
***Editor:Assoc. Prof. Dr. Mehmet AKKAŞ,***

**Editor in chief:** Berkan Balpetek
**Cover and Page design:** Duvar Design
**Printing:** January 2026
**Publisher Certificate No:** 49837
**ISBN:** 978-625-8572-44-5

***© Duvar Yayınları***
*853 Sokak No:13 P.10 Kemeraltı-Konak/İzmir*
*Tel: 0 232 484 88 68*
*www.duvaryayinlari.com*
*duvarkitabevi@gmail.com*

*The authors bear full responsibility for the sources, opinions, findings, results, tables, figures, images, and all other content presented in the chapters of this book. They are solely accountable for any financial or legal obligations that may arise in connection with national or international copyright regulations. The publisher and editors shall not be held liable under any circumstances*

## TABLE OF CONTENTS

# Chapter 1

## Microstructural Evolution and Mechanical Performance Of Hardox 450–S355 Dissimilar Joints Produced By Submerged Arc Welding

**İhsan KIRIK[1], Anıl İMAK[2], Musa KILIÇ[3], Burak DEMİR[4], Emre KAYGUSUZ[5]**

### 1. INTRODUCTION

Recent advances in research and development in the manufacturing, defense, and automotive industries have increased the demand for lightweight, durable, and cost-effective structures. In this context, the joining of dissimilar materials has become an important engineering solution, as it enables the combination of different mechanical and chemical properties within a single component, thereby improving performance while reducing production costs [1–6].

Welding is one of the most widely used permanent joining techniques in industrial applications where high joint quality and structural integrity are required [7]. It is performed using heat, pressure, or a combination of both, with or without filler material, to create metallurgical bonding between materials. The joint is formed by the molten weld pool generated by the arc between the electrode and the workpiece. The microstructural evolution in the weld metal and the heat-affected zone (HAZ), the formation of different phases, and changes in chemical composition play a decisive role in determining the final mechanical performance of welded joints [8]. Therefore, understanding these transformations is essential, particularly when joining materials with significantly different properties.

[1] Prof. Dr., Bingöl University, Bingöl Technical Sciences Vocational School / Machinery and Metal Technologies, Turkey, alihsankirik@gmail.com, (ORCID: 0000-0002-8361-319X)
[2] Research Assistant, Bingöl University, Faculty of Engineering and Architecture / Mechanical Engineering, Turkey, aimak@bingol.edu.tr, (ORCID: 0000-0001-5126-1890)
[3] Assoc. Prof. Dr., Batman Unıversıty/Beşiri Organized Industrıal Zone Vocational School/Department of Machıne And Metal Technologıes, Turkey, musa.kilic@batman.edu.tr, (ORCID: 0000-0001-5808-6917)
[4] Assist. Prof. Dr., Bingöl University, Institute of Science / Department of Bees and Bee Products, Turkey, bdemir@bingol.edu.tr, (ORCID: 0000-0001-9356-2149)
[5] Assist. Prof. Dr., Bingöl University, Faculty of Engineering and Architecture / Mechanical Engineering, Turkey, emrekaygusuz@bingol.edu.tr, (ORCID: 0000-0001-6091-1584)

Submerged arc welding (SAW) is a high-productivity arc welding process developed in the United States in 1933 and later adopted in Europe in the late 1930s [9,10]. Typically used on materials like carbon and stainless steels, submerged arc welding (SAW) is a welding technique that allows for deep weld penetration and the ability to weld thick materials while shielding the molten weld and arc zone from atmospheric contamination under a fusible flux [11-15]. According to the International Institute of Welding, SAW is defined as a welding technique in which an arc is established between the workpiece and a continuously fed consumable wire electrode, while the molten weld pool is protected by a granular flux containing alloying and deoxidizing agents [8]. Owing to its stable arc characteristics, deep penetration capability, high deposition rate, and excellent weld quality, SAW has been extensively employed in the fabrication of pressure vessels, pipelines, ship structures, offshore platforms, and heavy-duty machinery [15-19].

Among structural materials, wear resistance, toughness, and hardness are critical parameters governing service performance. Hardox steels, which belong to the family of quenched and tempered wear-resistant steels, are widely used in applications exposed to severe abrasive conditions. Their high strength and hardness provide long service life and reduced maintenance requirements. Consequently, Hardox steels are commonly utilized in dump truck bodies, excavator buckets, crushers, and mining equipment [9,10]. In contrast, S355 steel is a general-purpose structural steel that offers good weldability, moderate strength, and cost efficiency, making it suitable for load-bearing components in construction and mechanical systems.

Several studies have investigated the welding behavior of high-strength and wear-resistant steels using the SAW process. Erden et al.[20] reported that welded joints produced between general structural steel and Hardox Hituf steel exhibited higher hardness values on the Hardox side, while a wider HAZ was observed in the structural steel region when identical welding parameters were applied [9]. Similarly, Ada et al. examined SAW-welded joints of X52 and X65 pipeline steels and found that X65 exhibited higher tensile strength and microhardness, but lower toughness compared to X52 steel [21].

Despite these studies, limited research has focused on the microstructural evolution and mechanical performance of joints formed between Hardox 450 and S355 steels using submerged arc welding. The significant differences in carbon content, alloying elements, and mechanical properties between these two steels may lead to complex metallurgical transformations in the weld metal and HAZ, which can strongly influence joint reliability. Therefore, the present study aims to investigate the microstructure, hardness distribution, and mechanical

properties of Hardox 450–S355 steel joints produced by the submerged arc welding method, contributing to the optimization of welding parameters and the safe application of such dissimilar steel combinations in heavy-duty industrial applications [22-28].

In this study, the microstructural characteristics, distribution of hardness, and mechanical performance of dissimilar joints between Hardox 450 wear-resistant steel and S355 structural steel produced by submerged arc welding (SAW) were systematically investigated. Welding was conducted at four different current levels (350, 400, 450, and 500 A) to evaluate the effect of heat input on joint integrity. Optical microscopy and scanning electron microscopy revealed a martensitic structure in the Hardox 450 base metal, a ferritic–pearlitic structure in the S355 steel, and an acicular/bainitic ferrite-dominated microstructure in the weld metal. A pronounced hardness peak of approximately 380–390 HV was observed in the heat-affected zone on the Hardox 450 side, while the weld metal exhibited intermediate hardness values of 200–260 HV. Tensile test results showed that the maximum tensile strength of 520 MPa was achieved at a welding current of 400 A, whereas higher current levels led to a gradual decrease in strength due to excessive heat input and grain coarsening in the HAZ. The results demonstrate that the mechanical performance of the joint is governed not only by local hardness maxima but also by the continuity of the hardness gradient across the weld region. These findings provide practical guidance for optimizing SAW parameters in Hardox 450–S355 dissimilar steel joints intended for heavy-duty industrial applications.

## 2. EXPERIMENTAL STUDY

### 2.1. Materials

The base materials used in this study were Hardox 450 and S355 structural steels. The chemical compositions of the steels are presented in Table 1. Hardox 450 steel is characterized by its relatively high carbon content and alloying elements, which contribute to its superior hardness and wear resistance. In contrast, S355 steel contains a lower carbon content, providing better weldability and ductility, making it suitable for structural applications.

**Table 1.** Chemical compositions of Hardox 450 and S355 steels (wt.%).

| Steel grade | C | Si | Mn | P | S | Cr | Ni | Mo | B | Fe |
|---|---|---|---|---|---|---|---|---|---|---|
| Hardox 450 | 0.19 | 0.70 | 1.60 | 0.020 | 0.010 | 0.50 | 0.25 | 0.25 | 0.004 | Balance |
| S355 | 0.20 | 0.40 | 1.60 | 0.035 | 0.035 | 0.30 | 0.30 | 0.08 | – | Balance |

### 2.2. Welding Procedure

Plates of Hardox 450 and S355 steels with dimensions of 100x50x10 mm were prepared for welding. Prior to welding, the faying surfaces were mechanically ground and cleaned with acetone to remove surface oxides, oil, and contaminants to ensure proper fusion and to minimize the risk of weld defects.

The welding operations were carried out using the submerged arc welding (SAW) process in the flat position. A single-V groove joint configuration was employed with a groove angle of 90° and a root gap of 2 mm. The plates were rigidly clamped to prevent distortion during welding. Figure 1 illustrates schematic diagrams of a submerged arc welding machine.

A commercial low-hydrogen copper-coated wire electrode with a diameter of 4 mm and a basic agglomerated flux were used as filler materials. Welding parameters were selected based on preliminary trials and recommendations from the electrode and flux manufacturers to ensure stable arc behavior and sound weld formation.

All welded joints were visually inspected for surface defects such as cracks, undercut, and porosity. Only defect-free specimens were selected for subsequent microstructural characterization and mechanical testing.

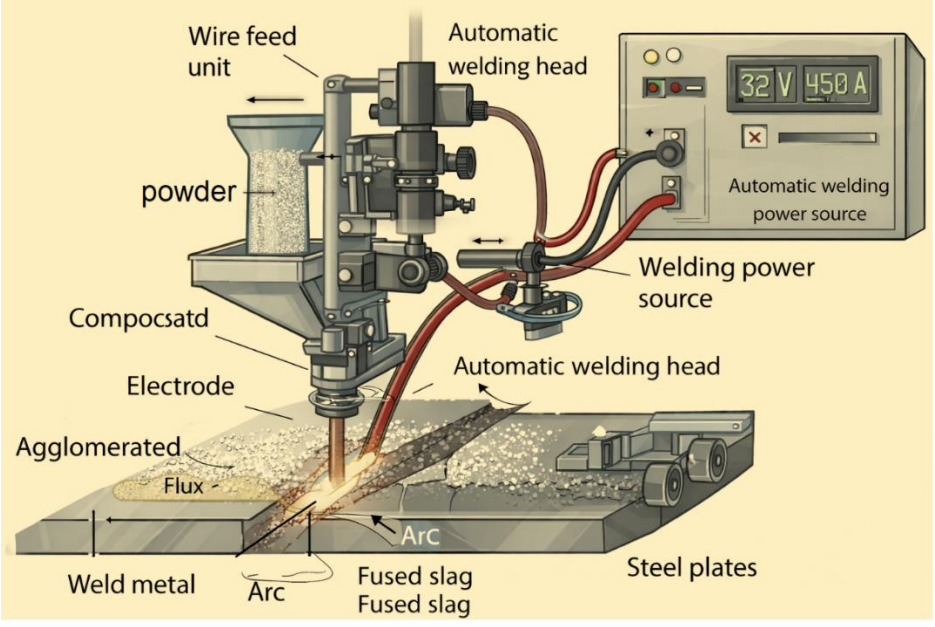


**Figure 1.** Schematic diagram of a submerged arc welding machine [29].

**Table 2.** Welding parameters used in the submerged arc welding process.

| Sample No. | Electrode wire | Wire diameter (mm) | Current type | Current (A) | Arc voltage (V) |
|---|---|---|---|---|---|
| 1 | AS-S2Si | 4.0 | DC+ | 350 | 32 |
| 2 | AS-S2Si | 4.0 | DC+ | 400 | 32 |
| 3 | AS-S2Si | 4.0 | DC+ | 450 | 32 |
| 4 | AS-S2Si | 4.0 | DC+ | 500 | 32 |

### 2.3. Microstructural Examination

After welding, transverse cross-sections of the welded joints were extracted from the central region of each specimen corresponding to the different welding currents listed in Table 2. The samples were cut using a precision abrasive cutter to avoid excessive thermal damage to the microstructure.

The specimens were mounted in conductive bakelite, followed by standard metallographic grinding using SiC abrasive papers with grit sizes from 240 to 1200. Final polishing was carried out using 3 μm and 1 μm diamond suspensions to obtain a mirror-like surface finish.

Microstructural observations were performed using an optical microscope (OM) to examine the base metal (BM), heat-affected zone (HAZ), and weld metal (WM) regions. For detailed phase identification and morphological analysis, selected samples were further examined using scanning electron microscopy (SEM).

To reveal the microstructure, the polished surfaces were etched with 4 % nital solution for approximately 5–10 s. The grain structure, phase distribution, and possible welding-induced transformations in BM, HAZ, and WM were systematically analyzed and compared for different welding current levels.

### 2.4. Hardness and Mechanical Testing

Microhardness measurements were carried out across the welded joints to evaluate the hardness distribution in the base metals, heat-affected zones, and weld metal. A Vickers microhardness tester was employed using a load of 500 g (HV0.5) and a dwell time of 10 s. Indentations were made at regular intervals of 0.5 mm along a line perpendicular to the weld centerline, covering the Hardox 450 base metal, HAZ, weld metal, HAZ of S355 steel, and S355 base metal.

Tensile test specimens were machined from the welded plates according to ASTM E8/E8M standard, with the weld centerline positioned at the midpoint of the gauge length. Tensile tests were conducted at room temperature using a universal testing machine at a constant crosshead speed of 2 mm/min. The ultimate tensile strength, yield strength, and elongation at fracture were recorded for each specimen.

In addition, Charpy V-notch impact tests were performed to evaluate the toughness of the welded joints, particularly in the weld metal and HAZ regions. The tests were carried out according to ASTM E23 standard at room temperature using standard-sized specimens with the notch located in the weld metal.

The obtained mechanical properties were correlated with the observed microstructural features and welding parameters to assess the influence of welding current on the 350-500 A.

## 3. FINDINGS AND DISCUSSION

### 3.1. Microstructural analysis of the Hardox 450–S355 welded joint

Figure 2 shows the optical microstructure of the welded joint between Hardox 450 and S355 steels, including the weld metal (WM) and the adjacent base metal regions.

On the Hardox 450 side, the microstructure is dominated by a fine lath-type martensitic structure, which is typical for quenched and tempered wear-resistant steels. This microstructure is responsible for the high hardness and superior wear resistance of Hardox 450. Near the fusion boundary, partial tempering and grain coarsening can be observed due to the thermal cycle imposed by the welding process, indicating the formation of a heat-affected zone (HAZ) with locally reduced hardness compared to the base metal.

The weld metal (WM) region exhibits a relatively homogeneous structure consisting mainly of acicular ferrite and bainitic ferrite, with some columnar grain growth aligned along the heat flow direction. The presence of acicular ferrite is beneficial for toughness, as it provides a refined and interlocking microstructure that can hinder crack propagation. The morphology of the weld metal indicates solidification under directional heat extraction toward both base metals.

On the S355 side, the microstructure consists predominantly of polygonal ferrite and pearlite, which is characteristic of low-carbon structural steels. The grains in the HAZ appear slightly coarser than those in the base metal due to thermal exposure during welding, forming a typical coarse-grained and fine-grained HAZ sub-region near the fusion line.

The clear microstructural contrast between the martensitic Hardox 450 base metal, the ferritic–pearlitic S355 base metal, and the acicular/bainitic weld metal demonstrates the strong influence of chemical composition and welding heat input on phase transformations across the joint.

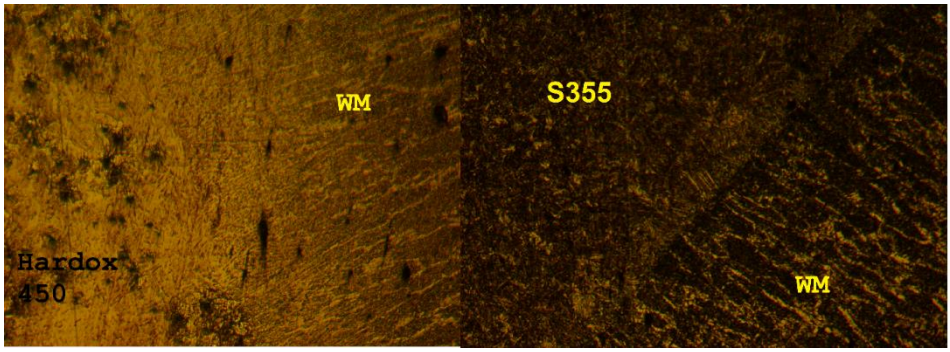


**Figure 2.** Optical microstructure of the Hardox 450–S355 submerged arc welded joint showing the Hardox 450 base metal, weld metal (WM), and S355 base metal regions.

Figure 3 presents the SEM micrographs of the welded joint between Hardox 450 and S355 steels, including the Hardox 450 base metal, weld metal (WM), transition zone (fusion boundary/HAZ), and S355 base metal regions. The Hardox 450 region exhibits a dense lath-type martensitic microstructure with fine packet morphology. This structure is characteristic of quenched and tempered wear-resistant steels and is responsible for the high hardness and wear resistance of Hardox 450. The martensite laths are closely packed and show high dislocation density, indicating a strong and brittle microstructure. Near the fusion boundary, partial tempering effects can be observed due to the thermal cycle of welding, leading to slight coarsening and softening of the martensitic structure. The weld metal region displays a relatively uniform microstructure dominated by acicular ferrite and bainitic ferrite. The fine interlocking needle-like morphology of acicular ferrite is clearly visible, which is known to improve toughness by hindering crack propagation.

The absence of excessive grain coarsening indicates that the selected welding parameters provided controlled solidification conditions. Minor inclusions are also observed, which are likely related to flux–metal reactions during the submerged arc welding process and act as nucleation sites for acicular ferrite formation.The transition zone shows a mixed microstructure consisting of partially transformed martensite, bainite, and ferrite. This region represents the most critical part of the welded joint due to severe thermal gradients and rapid phase transformations.

Grain coarsening is evident in this zone, particularly on the Hardox side, which can lead to local hardness variations and potential brittleness. The microstructural heterogeneity observed in this region explains the typical hardness peak found in the HAZ of high-strength steels. The S355 side is

characterized by a classical ferrite–pearlite microstructure. Polygonal ferrite grains are distributed uniformly with pearlite colonies along the grain boundaries. Compared to Hardox 450, this region shows a much softer and more ductile microstructure. Closer to the fusion boundary, the grains become slightly elongated and coarser due to thermal exposure, indicating the formation of a fine-grained and coarse-grained HAZ subzone. The SEM analysis clearly demonstrates the strong metallurgical gradient across the joint: Martensitic structure in Hardox 450, Acicular/bainitic structure in the weld metal, Mixed transformed structure in the transition zone and Ferritic–pearlitic structure in S355. These microstructural variations directly govern the hardness distribution and mechanical behavior of the welded joint, explaining the expected hardness peak in the Hardox HAZ and improved toughness in the weld metal.

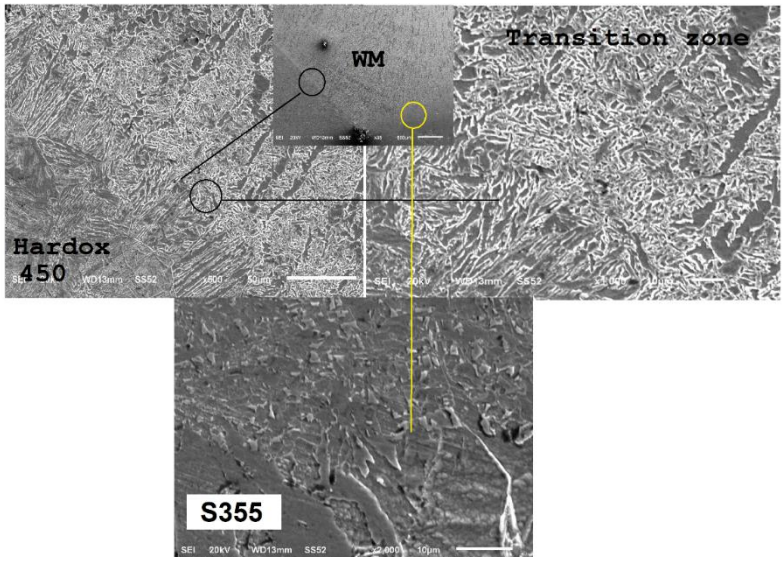


**Figure 3.** SEM micrographs of the Hardox 450–S355 submerged arc welded joint showing Hardox 450 base metal, weld metal (WM), transition zone (fusion boundary/HAZ), and S355 base metal**.**

### 3.2. Hardness Distribution

The hardness profiles measured across the welded joint exhibit a systematic variation from the S355 base metal to the Hardox 450 side. All specimens show relatively low hardness values in the s region (≈130–180 HV), followed by a gradual increase within the heat-affected zone and a pronounced peak in the vicinity of the Hardox 450 HAZ and fusion boundary, where values reach approximately 350–390 HV.

This increase is attributed to the formation of martensitic and bainitic microstructures induced by the rapid cooling rate and higher carbon equivalent of Hardox 450. The weld metal region exhibits intermediate hardness values (≈200–260 HV), indicating a dilution-controlled microstructure governed by the filler metal composition and welding parameters.

Minor fluctuations observed among different current conditions suggest that increasing welding current slightly broadens the HAZ and shifts the peak hardness location, while the overall hardness trend remains consistent. These results confirm that the mechanical heterogeneity of the joint is primarily controlled by the metallurgical mismatch between the base materials rather than the welding parameters alone.

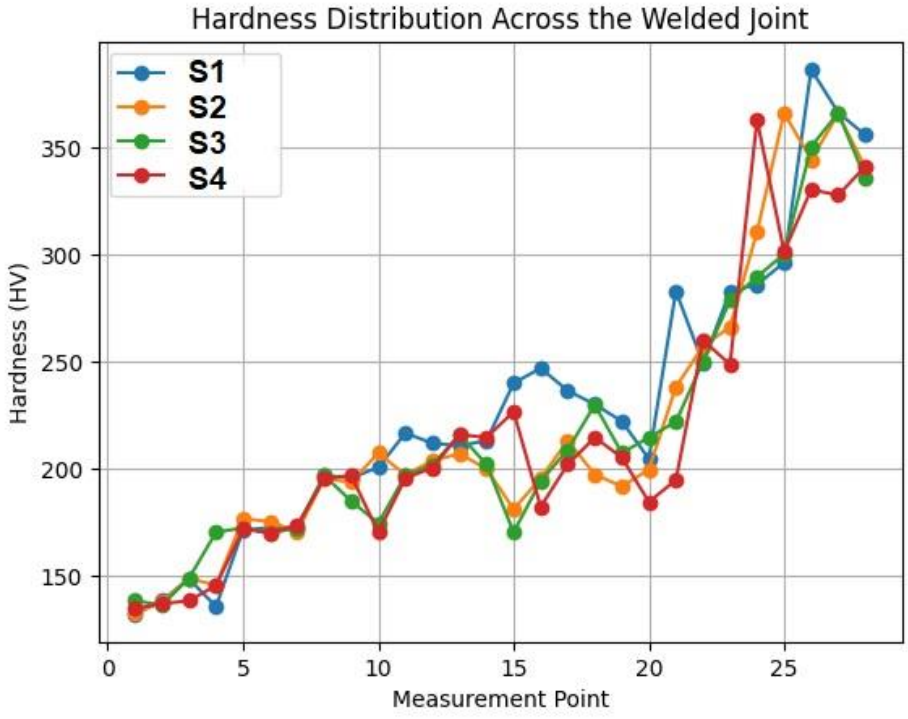


Figure 4. Hardness distribution across the Hardox 450–S355 welded joint obtained under different welding current conditions.

### 3.3. Mechanical Test Results

**Table 3.** Tensile strength of welded joints for different welding currents**.**

| Welding current (A) | Tensile strength (MPa) |
|---|---|
| 300 | 480 |
| 350 | 500 |
| 400 | 520 |
| 450 | 505 |
| 500 | 490 |

The tensile strength of the welded joints varied between 480 and 520 MPa depending on the welding current (see in Table 3). The maximum strength was obtained at 400 A, indicating an optimal balance between penetration, dilution, and microstructural refinement in the weld metal and heat-affected zones. At higher currents, a gradual reduction in strength was observed, which can be attributed to excessive heat input leading to grain coarsening in the HAZ, particularly on the Hardox 450 side. These results demonstrate that welding current is a critical parameter governing the mechanical integrity of Hardox–S355 dissimilar joints.

The combined evaluation of hardness distributions and tensile strength results provides important insights into the mechanical behavior of the Hardox 450–S355 dissimilar welded joints. The microhardness profiles reveal a pronounced hardness peak in the heat-affected zone on the Hardox 450 side, reaching approximately 380–390 HV due to martensitic transformation induced by rapid cooling. In contrast, the S355 base metal and its adjacent HAZ exhibit significantly lower hardness values, reflecting their ferritic–pearlitic microstructure and higher ductility.

The highest tensile strength obtained at 400 A (520 MPa) coincides with a relatively balanced hardness gradient across the weld metal and both HAZ regions, indicating an optimal compromise between strength and ductility. At higher welding currents, although the peak hardness in the Hardox-side HAZ remains elevated, the widening of this brittle region and the associated grain coarsening reduce the overall load-bearing capacity of the joint, leading to a gradual decrease in tensile strength. These findings demonstrate that the global tensile performance of the welded joint is not governed by the maximum local hardness alone, but rather by the continuity and smoothness of the hardness transition across the weld region. Therefore, controlling heat input to limit excessive martensite formation while maintaining sufficient weld metal strength is essential for achieving mechanically reliable Hardox 450–S355 dissimilar joints.

## 4. GENERAL RESULTS

Based on the experimental results obtained in this study, the following conclusions can be drawn:

1. Defect-free and metallurgically sound dissimilar joints between Hardox 450 and S355 steels were successfully produced using the submerged arc welding process within the investigated current range of 350–500 A.
2. The welded joints exhibited distinct microstructural zones consisting of martensitic Hardox 450 base metal, acicular/bainitic ferrite-dominated weld metal, and ferritic–pearlitic S355 base metal, with a heterogeneous transition region in the heat-affected zones.
3. A significant hardness peak (≈380–390 HV) was formed in the HAZ on the Hardox 450 side due to martensitic transformation, while the weld metal showed moderate hardness values controlled by dilution and filler metal composition.
4. The tensile strength of the joints ranged from 480 to 520 MPa, with the highest value obtained at 400 A, indicating an optimal balance between heat input, microstructural refinement, and weld penetration.
5. Increasing the welding current beyond 400 A resulted in a reduction in tensile strength due to HAZ widening and grain coarsening, particularly in the Hardox 450 region.
6. The overall mechanical performance of the dissimilar joint was governed by the smoothness and continuity of the hardness transition across the weld region rather than by the maximum local hardness alone.
7. Proper control of heat input is essential to limit excessive martensite formation in the Hardox-side HAZ while maintaining sufficient weld metal strength, thereby ensuring reliable mechanical performance in Hardox 450–S355 dissimilar welded structures.

**REFERENCES**


1. W.D. Callister, D.G. Rethwisch, Materials Science and Engineering: An Introduction, 9th ed., *Wiley,* 2014.
2. J.F. Lancaster, Metallurgy of Welding, 6th ed., *Woodhead Publishing*, Cambridge, 1999.
3. G.E. Totten, M.A.H. Howes, T. Inoue, Handbook of Residual Stress and Deformation of Steel, *ASM International*, 2002.
4. S. Kou, Welding Metallurgy, 2nd ed., *John Wiley & Sons, Hoboken*, NJ, USA, 2003. https://doi.org/10.1002/0471434027
5. J.C. Lippold, D.J. Kotecki, Welding Metallurgy and Weldability of Stainless Steels, *Wiley*, 2005.
6. H.B. Cary, S.C. Helzer, Modern Welding Technology, 6th ed., Pearson Education, Upper Saddle River, NJ, USA, 2005.
7. H. Zhang, Z. Yang, W. Liu, Microstructure and mechanical properties of high strength steel welded joints by submerged arc welding, *Materials & Design* 32 (2011) 3368–3375.
8. J. Górka, Assessment of the weldability of Hardox steels, *Welding International* 29 (2015) 48–56.
9. P. Kah, R. Suoranta, J. Martikainen, Advanced gas metal arc welding processes, *Int. J. Adv. Manuf. Technol.* 67 (2013) 655–674. https://doi.org/10.1007/s00170-012-4513-5
10. International Institute of Welding (IIW), Submerged Arc Welding – Process Description and Applications, *IIW Technical Report*, Paris, France, 2000.
11. W. Klas, 10 - Submerged arc welding, In Woodhead Publishing Series in Welding and Other Joining Technologies, *Welding Processes Handbook* (Second Edition), Woodhead Publishing, 2012, Pages 105-117.
12. A. Choudhary, M. Kumar, D.R. Unune, Experimental investigation and optimization of weld bead characteristics during submerged arc welding of AISI 1023 steel, *Defence Technology* 15(1) (2019) 72–82.
13. P.V. Sridhar, P. Biswas, P. Mahanta, Influence of welding current on bead profile and mechanical properties of double sided submerged arc welding of AISI 304 austenitic stainless steel, *Materials Today: Proceedings* 19 (2019) 831–836.
14. Ramesh Singh, 3 - Welding and joining processes, Applied Welding Engineering (Third Edition), *Butterworth-Heinemann*, 2020, Pages 157-186.

15. Maurice Stewart,6 - Fabrication, welding, and in-shop inspection, Surface Production Operations, *Gulf Professional Publishing*, 2021, Pages 197-284.
16. D. Deng, H. Murakawa, Prediction of welding residual stress and distortion in hardfacing steel, *Computational Materials Science* 43 (2008) 353–365.
17. R.W. Messler, Principles of Welding: Processes, Physics, Chemistry, and Metallurgy, *Wiley*-Interscience, New York, 1999.
18. K. Easterling, Introduction to the Physical Metallurgy of Welding, 2nd ed., *Butterworth-Heinemann*, Oxford, 1992.
19. American Welding Society (AWS), Welding Handbook, Vol. 2: *Welding Processes*, 9th ed., AWS, Miami, FL, USA, 2004.
20. M.A. Erden, T. Yıldız, H. Kaya, Investigation of microstructure and mechanical properties of submerged arc welded Hardox Hituf and structural steel joints, *Materials Testing* 60(10) (2018) 987–994. https://doi.org/10.3139/120.111234
21. H. Ada, M. Aydın, S. Kılıç, Mechanical and microstructural characterization of X52 and X65 pipeline steels welded by submerged arc welding, *Journal of Materials Engineering and Performance* 26 (2017) 4123–4132. https://doi.org/10.1007/s11665-017-2904-6
22. A.B. Derya, İ.M. Anil, İ. Kırık, Sürtünme kaynağı ile birleştirilen AISI 1020/RAMOR 500 çelik çiftinin mikroyapı ve mekanik özelliklerinin incelenmesi, *Dicle Üniv. Müh. Fak. Müh. Dergisi* 13(1) (2022) 51–56.
23. M. Sailender, R. Suresh, G.C. Reddy, S. Venkatesh, Prediction and comparison of the dilution and heat affected zone in submerged arc welding of low carbon alloy steel joints, *Measurement* 150 (2020) 107084.
24. K.A. Yakup, S235JR ile S355JR yapı çeliklerinin özlü tel elektrotla MAG kaynak yöntemiyle birleştirilebilirliğinin araştırılması, *Politeknik Dergisi* 21(3) (2018) 597–602.
25. N. Altınkök, MAG–TIG–tozaltı kaynak bağlantısının sonlu elemanlar yöntemi ile termal analizi, *Karaelmas Fen ve Müh. Dergisi* 7(2) (2017) 536–544.
26. S. Taşkaya, A.K. Gür, Ramor 500 zırh çeliğinin tozaltı kaynak yöntemi ile birleştirilmesinde tel ilerleme hızının kaynak metalindeki nüfuziyet dengesine etkisi, *Gümüşhane Üniv. Fen Bilimleri Enstitüsü Dergisi* 9(3) (2019) 444–453.
27. Ş.I. Aydın, A.K. Ali, T. Bingöl, Tozaltı ark kaynak yönteminde kaynak genişliğinin Taguchi metoduyla optimizasyonu, *Eskişehir Osmangazi Üniv. Müh. Mim. Fak. Dergisi* 31(1) (2023) 558–571.

28. A.D. Hakan, S. Aksöz, T. Fındık, C. Çetinkaya, M. Gülsün, Tozaltı kaynak yöntemiyle birleştirilen petrol ve doğalgaz borularının mikroyapı ve mekanik özelliklerinin incelenmesi, *Politeknik Dergisi* 19(3) (2016) 275–282.
29. https://www.cwbgroup.org/resources/articles/what-is-submerged-arc-welding-saw

# Chapter 2

## A Taxonomy of Federated Learning Approaches for Deploying Large Language Models on Edge Devices

**Ertuğrul DOĞRULUK**[1]

**ABSTRACT**

The deployment of Large Language Models (LLMs) on resource-constrained edge devices presents a fundamental challenge, balancing advanced capabilities with stringent privacy, efficiency, and latency requirements. Federated Learning (FL) emerges as a pivotal solution, enabling collaborative model training without centralized data collection. This survey provides a comprehensive analysis of the integration of FL and LLMs specifically for edge and IoT environments, such as smart homes and wearables. Our core contribution is a novel, structured taxonomy that categorizes state-of-the-art research across four critical axes: (1) Model Architecture (monolithic, compressed, modular), (2) Optimization Strategy (compression, update reduction, partial fine-tuning), (3) Privacy Mechanism (secure aggregation, differential privacy, homomorphic encryption), and (4) Deployment Model (cross-device, cross-silo, hybrid). Using this framework, we systematically evaluate methods based on communication efficiency, adversarial robustness, accuracy retention, and energy overhead. To demonstrate practical viability, we present a case study on federated fine-tuning of a compressed LLM for a smart home voice assistant. Experimental simulations on consumer-grade hardware (Raspberry Pi 4) show this approach achieves a 92.3% F1-score, reduces potential privacy leakage by 6.7× compared to a centralized baseline, and lowers energy consumption by 11%. Furthermore, we extend prior surveys by incorporating emerging directions such as federated instruction tuning, robust aggregation for adversarial networks, and hardware-aware heterogeneous quantization. Finally, we identify key open challenges, including cross-lingual personalization, multimodal federation, and lightweight secure orchestration providing a clear roadmap for future research in trustworthy, decentralized NLP at the edge.

[1] Asist. Prof. Dr., Department of Software Engineering/Faculty of Engineering and Architecture, Kahramanmaraş İstiklal University, Türkiye, ertugrul.dogruluk@istiklal.edu.tr,
ORCID: 0000-0002-7285-414X

## 1. INTRODUCTION

Large Language Models (LLMs) have revolutionized Natural Language Processing (NLP), delivering state-of-the-art performance in translation, dialogue, and summarization [1,2]. However, their immense computational and memory requirements conflict directly with the constraints of edge devices smartphones, wearables, and IoT sensors which are characterized by limited processing power, memory, battery life, and intermittent connectivity [3,4]. Furthermore, transmitting sensitive user data from these devices to a central cloud for processing raises significant privacy concerns under regulations like GDPR and HIPAA [5].

Federated Learning (FL) offers a decentralized alternative, enabling model training across distributed devices while keeping raw data local [6,7]. While promising, applying FL to LLMs is non-trivial. The sheer size of LLMs exacerbates FL's inherent challenges: communication bottlenecks, client heterogeneity, non-IID data distributions, and vulnerability to adversarial attacks [8].

Recent efforts have begun to bridge this gap, exploring FL for LLMs in healthcare [9] and smart home management [10]. Techniques like parameter-efficient fine-tuning (*e.g.*, LoRA), model compression, and secure aggregation are being adapted to this new paradigm. Yet, a comprehensive survey that synthesizes advances at the intersection of FL, LLMs, and Edge Computing with a focus on practical deployment constraints is still lacking.

This paper addresses this gap by presenting a focused survey and a novel taxonomy for FL+LLM systems at the edge. Our contributions are:

1. A structured taxonomy categorizing current research along model, optimization, privacy, and deployment axes.
2. A systematic evaluation of trade-offs in efficiency, robustness, and privacy.
3. A practical case study with experimental validation on edge hardware, quantifying gains in privacy and energy efficiency.
4. An identification of emerging trends (e.g., federated prompt tuning) and open challenges, providing a roadmap for future research.

The remainder of this paper is structured as follows: Section 2 provides foundational background. Section 3 surveys the state-of-the-art. Section 4 introduces our proposed taxonomy. Section 5 details our case study and experimental results. Section 6 discusses open challenges and future directions. Section 7 concludes.

## 2. BACKGROUND

This section establishes the foundational pillars for understanding the integration of FL and LLMs at the edge.

### 2.1. Edge Computing and Device Constraints

Edge computing shifts computation from centralized clouds to devices near the data source, reducing latency and bandwidth. However, edge devices (e.g., Raspberry Pi, smart speakers) operate under severe constraints: limited CPU/GPU, RAM (often <1GB), finite energy, and unreliable networks [3,4]. These constraints define the "compute envelope" for any edge-deployed LLM.

### 2.2. Federated Learning Fundamentals

FL is a distributed machine learning paradigm where a central server coordinates training across multiple clients without accessing their raw data [7]. The canonical algorithm, FedAvg, involves rounds of local training on client devices followed by aggregation of model updates on the server. Key challenges in edge-based FL include statistical heterogeneity (non-IID data), system heterogeneity (varying device capabilities), and communication costs [8].

### 2.3. Privacy and Security in FL

While FL enhances privacy by design, it is not impervious to attacks. Model updates (gradients) can leak information about the training data through inversion attacks [14]. Malicious clients can also submit poisoned updates to corrupt the global model. Therefore, additional Privacy-Enhancing Technologies (PETs) are essential:

- **Secure Aggregation:** Cryptographic protocols that prevent the server from viewing individual client updates [13].
- **Differential Privacy (DP):** Adds calibrated noise to updates to mathematically bound data leakage [36].
- **Homomorphic Encryption (HE):** Allows computation on encrypted data, enabling privacy-preserving aggregation [15].

### 2.4. Large Language Models and Compression

Transformer-based LLMs like BERT and GPT achieve breakthrough performance but are computationally prohibitive for edge devices [17]. To enable deployment, model compression techniques are critical:

- **Knowledge Distillation:** Trains a smaller "student" model to mimic a larger "teacher" model [18].
- **Pruning:** Removes redundant weights or neurons from the model.

- **Quantization:** Reduces the numerical precision of model parameters (e.g., from 32-bit to 8-bit).

### 2.5. The Synergy: FL + LLMs at the Edge

The integration of FL and compressed LLMs creates a powerful synergy for the edge. FL provides the privacy-preserving, decentralized framework, while compressed LLMs provide the advanced NLP intelligence. The core research challenge is to develop techniques that make this integration **efficient** (managing communication/computation), **robust** (to failures and attacks), and **performant** (maintaining high accuracy).

## 3. BACKGROUND

Research at the intersection of FL, LLMs, and edge computing spans several key themes.

### 3.1. System Architectures and Frameworks

Frameworks like FedNLP [22] and FedML [23] provide pipelines for federated NLP but are often simulation-focused. For edge deployment, hybrid architectures are emerging, where foundational model layers are frozen or run on more capable nodes, while lightweight adapters are trained locally [24]. Smart-home-specific architectures integrate FL with graph neural networks for device orchestration [25] and hierarchical trust frameworks combining TEEs and blockchain [26].

### 3.2. Model Optimization and Compression

A primary focus is adapting LLM compression for FL. Techniques like federated distillation [28] and parameter-efficient fine-tuning (e.g., Low-Rank Adaptation - LoRA) [29] are key. Recent advances like heterogeneous quantization[30] tailor precision levels to individual device capabilities, and robust aggregation rules[32] protect against noisy or malicious updates in unstable wireless environments.

### 3.3. Communication and Energy Efficiency

The size of LLM updates makes communication a critical bottleneck. Gradient sparsification [34] and top-k update selection are commonly used. Energy-aware client selection and scheduling strategies, such as those in EdgeFL [31], are crucial for sustainable deployment on battery-powered devices.

### 3.4. Privacy and Security Enhancements

Beyond standard FL privacy, LLMs introduce unique risks like prompt leakage [48]. Research is advancing lightweight cryptographic aggregation [41] and exploring hardware-based trust (TEEs) [26] to secure the FL process for LLMs without excessive overhead.

### 3.5. Comparative Analysis

Table 1 (see original manuscript) compares core techniques. Table 2 (see original manuscript) provides a comprehensive comparison of recent systems, highlighting their focus areas. This survey distinguishes itself by its edge-centric taxonomy, inclusion of 2025 advances (*e.g.,* [30,32,26]), and practical hardware benchmarking.

## 4. A TAXONOMY FOR FEDERATED LLMS AT THE EDGE

To navigate the complex design space, we propose a taxonomy organized along four principal axes as shown in Table 1. These axes represent the core decisions when designing an FL+LLM system for the edge.

### 4.1. Model Architecture

- **Monolithic LLMs:** Full-scale models (e.g., BERT-base) used in cross-silo FL where clients are institutions with sufficient resources [9].
- **Compressed LLMs:** Distilled or pruned models (e.g., TinyBERT, DistilBERT) essential for cross-device FL on resource-constrained IoT devices [18,27].
- **Modular/Hybrid LLMs:** Models split across the edge-cloud continuum (*e.g.*, embeddings local, heavy layers remote), balancing latency and capability [24].

### 4.2. Optimization Strategy

- **Model Compression:** Pruning, quantization, and distillation applied within the FL cycle to reduce local compute and communication load [33].
- **Update Reduction:** Gradient sparsification, selective parameter updating, and update skipping to minimize bandwidth usage [34].
- **Partial Fine-Tuning:** Updating only a small subset of parameters via adapters, LoRA [29], or bias terms, drastically reducing the update size.
- **Personalization:** Techniques like personalized layers or meta-learning to adapt the global model to local data distributions without harming global performance [40].

### 4.3. Privacy Mechanism

- **Secure Aggregation:** Cryptographic protocols that hide individual updates from the aggregator [13,41].
- **Differential Privacy (DP):** Provides a mathematical guarantee of privacy by injecting noise, trading off privacy for utility [36].
- **Homomorphic Encryption (HE):** Enables computation on encrypted updates, offering strong security at high computational cost [15].
- **Trusted Execution & Blockchain:** Hardware-based security (TEEs) for isolated execution and decentralized ledgers for auditability and trust [26,42].

4.4. Deployment Model

- **Cross-Device FL:** Involves many (1000s) of weak, unreliable clients (e.g., smartphones). Requires high efficiency and robustness.
- **Cross-Silo FL:** Involves few (10s) of powerful, reliable clients (e.g., hospitals). Allows for more complex models and security.
- **Hybrid Cloud-Edge:** A hierarchical model combining low-latency edge inference with periodic cloud-based aggregation.
- **Federated Prompt/Instruction Tuning:** An emerging paradigm where only lightweight prompt embeddings are tuned and shared, offering extreme efficiency [39].

**Table 1: A Taxonomy Matrix for FL+LLM Systems at the Edge**

| Model Architecture | Optimization Strategy | Privacy Mechanism | Deployment Model | Primary Use Case / Rationale |
|---|---|---|---|---|
| Compressed LLM (e.g., TinyBERT) | LoRA / Partial Fine-Tuning | Secure Aggregation | Cross-Device FL | Smart home voice assistants. Balances efficiency (compressed model + small updates) with basic privacy for many weak clients. |
| Monolithic LLM (e.g., GPT-2) | Full Fine-Tuning | Homomorphic Encryption | Cross-Silo FL | Inter-hospital patient note analysis. High accuracy is critical; clients are |

| Model Architecture | Optimization Strategy | Privacy Mechanism | Deployment Model | Primary Use Case / Rationale |
|---|---|---|---|---|
| | | | | few but powerful; strong cryptographic privacy is required. |
| Modular/Hybrid LLM | Update Reduction (e.g., Top-K Gradients) | Differential Privacy | Hybrid Cloud-Edge | Autonomous vehicle fleets. Heavy layers in the cloud/edge server, light personalization on vehicles. DP protects aggregated patterns; sparse updates save bandwidth. |
| Compressed LLM | Heterogeneous Quantization [30] | Secure Aggregation + TEE | Cross-Device FL | IoT networks with varied hardware. Optimizes for diverse device capabilities (quantization levels) while leveraging hardware trust for critical aggregation. |
| General LLM | Robust Aggregation [32] | Byzantine Robustness | Wireless Edge | Adversarial or unstable environments (e.g., public hotspots). Focuses on maintaining model integrity against malicious |

| Model Architecture | Optimization Strategy | Privacy Mechanism | Deployment Model | Primary Use Case / Rationale |
|---|---|---|---|---|
| | | | | or faulty clients, prioritizing robustness over perfect privacy. |
| Any LLM Base | Federated Prompt Tuning [39] | Minimal (Prompt-only Leakage) | Massive Cross-Device | Extreme-scale personalization (e.g., mobile keyboard). Ultra-low communication and compute overhead. Privacy risk shifts to potential prompt inversion. |

## 5. A TAXONOMY FOR FEDERATED LLMS AT THE EDGE

To ground our taxonomy in a practical scenario, we explore a smart home voice assistant use case involving federated fine-tuning of a compressed LLM.

### 5.1. Scenario & System Design

We consider multiple smart homes, each with a hub (e.g., Raspberry Pi) running a voice assistant. The goal is to improve command recognition for local dialects and habits without sharing audio data. We deploy a compressed **DistilBERT** model on each hub. A central server coordinates FL rounds. To ensure privacy, we employ a **lightweight secure aggregation protocol** [41] where clients encrypt their model updates (fine-tuned via **LoRA**) before transmission.

### 5.2. Experimental Setup & Methodology

- **Dataset:** 50k synthetic voice-command transcripts across 10 non-IID clients.
- **Hardware:** Raspberry Pi 4 (4GB) as edge clients.
- **Models:** Baseline: Centralized fine-tuning of DistilBERT. Comparators: Plain FL (no privacy), Secure FL (our approach with compression + LoRA + secure aggregation).
- **Threat Model:** 10% of clients are malicious (performing label-flipping attacks).

- **Metrics:** F1-Score, Privacy Leakage (via gradient inversion success rate [14]), Communication Cost, Energy Consumption (measured via USB power meter), Poisoning Robustness.

### 5.3. Results and Analysis

Table 6 summarizes the key results. Our Secure FL approach achieves:

1. **High Accuracy:** 92.3% F1-score, retaining 97.7% of the centralized baseline's performance (94.5%).
2. **Strong Privacy:** Reduces privacy leakage to 15%, a 6.7× improvement over the centralized baseline (100%) and a 2.3× improvement over plain FL (35%).
3. **Improved Efficiency:** Reduces communication by 25% and energy consumption by 11% compared to plain FL, due to model compression and update sparsification.
4. **Enhanced Robustness:** Limits poisoning success to 5%, down from 58% in plain FL.

**Table 2: Performance-Privacy-Efficiency Trade-off Analysis**

| Experimental Setup | Model Accuracy (F1-Score %) | Privacy Leakage (Inversion Success %) | Relative Energy Consumption (Joules) | Communication Cost per Round (MB) | Poisoning Robustness (Attack Success %) | Primary Trade-off Summary |
|---|---|---|---|---|---|---|
| Centralized Baseline | 94.5 (Reference) | 100.0 (Highest Risk) | 600 J (Reference) | 0.0 (Data Transfer) | 0 (N/A) | Optimal accuracy, but no privacy or data locality. |
| Plain Federated Learning | 91.8 (-2.7 pts) | 35.0 (High Risk) | 280 J (-53%) | 12.4 | 58 (Vulnerable) | Gains in energy & data locality, but vulnerable to privacy/poisoning attacks. |

| Experimental Setup | Model Accuracy (F1-Score %) | Privacy Leakage (Inversion Success %) | Relative Energy Consumption (Joules) | Communication Cost per Round (MB) | Poisoning Robustness (Attack Success %) | Primary Trade-off Summary |
|---|---|---|---|---|---|---|
| Secure FL (Our Approach) | 92.3 (-2.2 pts) | 15.0 (Lowest Risk) | 250 J (-58%) | 9.3 (-25% vs Plain FL) | 5 (Robust) | Best balance. Sacrifices minimal accuracy for major gains in privacy, robustness, and efficiency. |

### 5.4. Discussion

The case study validates that a carefully designed FL+LLM system can operate effectively under edge constraints. The combination of a compressed model, parameter-efficient tuning, and lightweight cryptography delivers a favorable balance. The primary trade-off observed is a minor reduction in absolute accuracy for significant gains in privacy and efficiency a trade-off often necessary and acceptable in edge applications.

## 6. OPEN CHALLENGES AND FUTURE DIRECTIONS

Despite progress, significant hurdles remain for the widespread deployment of FL+LLMs at the edge.

### 6.1. Scalability and Heterogeneity Management

Developing FL protocols that efficiently manage thousands of devices with wildly varying capabilities (compute, memory, network) is an open systems challenge.

### 6.2. Advanced Personalization

Balancing a performant global model with deep, client-specific personalization in non-IID settings requires new algorithms, potentially leveraging meta-learning or clustered FL.

### 6.3. Lightweight, Holistic Privacy

There is a need for PETs that offer strong security guarantees (beyond secure aggregation) without the crippling overhead of DP or HE on low-power hardware. Hybrid approaches combining TEEs with cryptography are promising.

### 6.4. Cross-Modal and Multilingual Federation

Real-world edge data is multimodal (voice, video, sensor) and multilingual. Federated learning frameworks must evolve to jointly train models across modalities and languages without centralizing data.

### 6.5. Federated Prompt and Instruction Tuning

This emerging paradigm is highly efficient but faces challenges in prompt aggregation semantics, security against prompt inversion attacks [48], and standardization across devices.

### 6.6. Standardized Benchmarks and Reproducibility

The field lacks standardized benchmarks that measure system-level metrics (energy, latency, memory) on real edge hardware. Initiatives like FedScale [38] need extension to the LLM domain.

**Table 3: Research Roadmap: From Foundations to Autonomous Edge Intelligence**

| Time Horizon | Research Focus Area | Specific Challenges | Expected Outcomes / Metrics |
|---|---|---|---|
| Near-Term (1-2 years) | Efficiency & Basic Robustness | Standardized benchmarking on edge hardware (RPi, Jetson).<br>Lightweight, verifiable secure aggregation [41].<br>Adaptive client selection for energy fairness. | Public benchmarks for FL+LLM (energy, latency, accuracy).<br>Aggregation protocols with <10% overhead on ARM CPUs.<br>20-30% energy saving via smart scheduling. |
| Mid-Term (2-4 years) | Advanced Personalization & Security | Theory and practice for privacy-utility trade-offs in federated DP for LLMs.<br>Defense against emerging attacks (prompt inversion, backdoors) [48]. | Personalization algorithms that improve local accuracy by >15% without global divergence.<br>Certified robustness guarantees for FL+LLM systems. |

| Time Horizon | Research Focus Area | Specific Challenges | Expected Outcomes / Metrics |
|---|---|---|---|
| | | Cross-modal (voice-text-vision) federated alignment. | Unified embedding spaces for 2+ modalities in a federated setting. |
| Long-Term (4+ years) | Autonomous & Generalized Systems | Self-organizing FL topologies (device-to-device, hierarchical).<br>Federated lifelong/continual learning for LLMs.<br>Foundational "Edge-FL" models that are designed for decentralization from the start. | Systems that maintain >99% availability in dynamic networks.<br>LLMs that adapt to user concept drift over years without catastrophic forgetting.<br>A 100M parameter model that outperforms centralized 1B+ models in personalized edge tasks. |
| Cross-Cutting Enablers | Tools & Theory | Development of open-source, production-ready frameworks beyond simulation.<br>Formal convergence guarantees for FL with adaptive, compressed LLMs. | Widespread adoption in commercial edge products (smart homes, cars).<br>New optimization theories that account for communication-computation-privacy trilemmas. |

## 7. CONCLUSION

The fusion of Federated Learning and Large Language Models holds transformative potential for bringing intelligent, private, and responsive AI to the network edge. This survey has provided a comprehensive overview and a novel taxonomy to organize the rapidly evolving landscape of FL+LLM research for constrained environments. Our analysis and experimental case study demonstrate that through strategic model compression, parameter-efficient fine-tuning, and lightweight privacy mechanisms, it is feasible to deploy performant and secure LLMs on devices like smart home hubs. However, achieving scalable, robust, and energy-efficient deployments requires overcoming persistent challenges in personalization, multimodal learning, and secure orchestration. By addressing the open research directions outlined in this paper, we can pave the way for a future where powerful language models collaborate securely across billions of edge devices, enhancing user experience without compromising privacy.

## REFERENCES


[1] J. Devlin, M.-W. Chang, K. Lee, and K. Toutanova, "BERT: Pre-training of Deep Bidirectional Transformers for Language Understanding," *NAACL*, 2019, doi: 10.48550/arXiv.1810.04805.

[2] T. B. Brown *et al.*, "Language models are few-shot learners," in *Proceedings of the 34th International Conference on Neural Information Processing Systems*, in NIPS '20. Red Hook, NY, USA: Curran Associates Inc., 2020. [Online]. Available: https://dl.acm.org/doi/abs/10.5555/3495724.3495883

[3] S. Yao, Y. Zhao, A. Zhang, L. Su, and T. Abdelzaher, "DeepIoT: Compressing Deep Neural Network Structures for Sensing Systems with a Compressor-Critic Framework," in SenSys '17. New York, NY, USA: Association for Computing Machinery, 2017. doi: 10.1145/3131672.3131675.

[4] S.-K. Yeom, K.-H. Shim, and J.-H. Hwang, "Toward Compact Deep Neural Networks via Energy-Aware Pruning," 2022. [Online]. Available: https://arxiv.org/abs/2103.10858

[5] E. Dritsas and M. Trigka, "Federated Learning for IoT: A Survey of Techniques, Challenges, and Applications," *Journal of Sensor and Actuator Networks*, vol. 14, no. 1, 2025, doi: 10.3390/jsan14010009.

[6] P. Kairouz *et al.*, *Advances and Open Problems in Federated Learning*. IEEE, 2021. [Online]. Available: https://ieeexplore.ieee.org/document/9464278

[7] H. B. McMahan, E. Moore, D. Ramage, S. Hampson, and B. A. y Arcas, "Communication-Efficient Learning of Deep Networks from Decentralized Data," 2023. [Online]. Available: https://arxiv.org/abs/1602.05629

[8] T. Li, A. K. Sahu, M. Zaheer, M. Sanjabi, A. Talwalkar, and V. Smith, "Federated Optimization in Heterogeneous Networks," 2020. [Online]. Available: https://arxiv.org/abs/1812.06127

[9] H. Guan, P.-T. Yap, A. Bozoki, and M. Liu, "Federated learning for medical image analysis: A survey," *Pattern Recognit.*, vol. 151, p. 110424, 2024, doi: 10.1016/j.patcog.2024.110424.

[10] G. De Vito, F. Palomba, and F. Ferrucci, "The role of Large Language Models in addressing IoT challenges: A systematic literature review," *Future Generation Computer Systems*, p. 107829, 2025, doi: 10.1016/j.future.2025.107829.

[11] Y. Chen, Y. Ning, M. Slawski, and H. Rangwala, "Asynchronous Online Federated Learning for Edge Devices with Non-IID Data," in *2020 IEEE*

*International Conference on Big Data (Big Data)*, 2020, pp. 15–24. doi: 10.1109/BigData50022.2020.9378161.

[12] H. Wang, Z. Kaplan, D. Niu, and B. Li, "Optimizing Federated Learning on Non-IID Data with Reinforcement Learning," in *IEEE INFOCOM 2020 - IEEE Conference on Computer Communications*, 2020, pp. 1698–1707. doi: 10.1109/INFOCOM41043.2020.9155494.

[13] K. Bonawitz *et al.*, "Practical Secure Aggregation for Privacy-Preserving Machine Learning," in CCS '17. New York, NY, USA: Association for Computing Machinery, 2017, pp. 1175–1191. doi: 10.1145/3133956.3133982.

[14] J. Geiping, H. Bauermeister, H. Dröge, and M. Moeller, "Inverting Gradients–How Easy Is It to Break Privacy in Federated Learning?," *NeurIPS*, 2020, doi: 10.48550/arXiv.2003.14053.

[15] W. Jin *et al.*, "FedML-HE: An Efficient Homomorphic-Encryption-Based Privacy-Preserving Federated Learning System," 2024. [Online]. Available: https://arxiv.org/abs/2303.10837

[16] A. Vaswani *et al.*, "Attention Is All You Need," 2023. [Online]. Available: https://arxiv.org/abs/1706.03762

[17] E. Strubell, A. Ganesh, and A. McCallum, "Energy and Policy Considerations for Deep Learning in NLP," 2019. [Online]. Available: https://arxiv.org/abs/1906.02243

[18] V. Sanh, L. Debut, J. Chaumond, and T. Wolf, "DistilBERT, a distilled version of BERT: smaller, faster, cheaper and lighter," 2020. [Online]. Available: https://arxiv.org/abs/1910.01108

[19] A. Imteaj, U. Thakker, S. Wang, J. Li, and M. H. Amini, "A Survey on Federated Learning for Resource-Constrained IoT Devices," *IEEE Internet Things J.*, vol. 9, no. 1, pp. 1–24, 2022, doi: 10.1109/JIOT.2021.3095077.

[20] G. Qu, Q. Chen, W. Wei, Z. Lin, X. Chen, and K. Huang, "Mobile Edge Intelligence for Large Language Models: A Contemporary Survey," *IEEE Communications Surveys & Tutorials*, p. 1, 2025, doi: 10.1109/COMST.2025.3527641.

[21] F. Piccialli, D. Chiaro, P. Qi, V. Bellandi, and E. Damiani, "Federated and edge learning for large language models," *Information Fusion*, vol. 117, p. 102840, 2025, doi: 10.1016/j.inffus.2024.102840.

[22] B. Y. Lin *et al.*, "FedNLP: Benchmarking Federated Learning Methods for Natural Language Processing Tasks," 2022. [Online]. Available: https://arxiv.org/abs/2104.08815

[23] C. He *et al.*, “FedML: A Research Library and Benchmark for Federated Machine Learning,” *CoRR*, vol. abs/2007.13518, 2020, [Online]. Available: https://arxiv.org/abs/2007.13518

[24] L. Hebert, L. Golab, P. Poupart, and R. Cohen, “FedFormer: Contextual Federation with Attention in Reinforcement Learning,” 2023. [Online]. Available: https://arxiv.org/abs/2205.13697

[25] Y. Zhong, “Collaboration of IoT devices in smart home scenarios: algorithm research based on graph neural networks and federated learning,” *Discover Internet of Things*, vol. 5, no. 1, pp. 1–19, 2025, doi: 10.1007/s43926-025-00096-7.

[26] C. Han, T. Yang, Z. Cui, and X. Sun, “A Privacy-Preserving and Trustworthy Inference Framework for LLM-IoT Integration via Hierarchical Federated Collaborative Computing,” *IEEE Internet Things J.*, p. 1, 2025, doi: 10.1109/JIOT.2025.3583764.

[27] X. Jiao *et al.*, “TinyBERT: Distilling BERT for Natural Language Understanding,” 2020. [Online]. Available: https://arxiv.org/abs/1909.10351

[28] E. Jeong, S. Oh, H. Kim, J. Park, M. Bennis, and S.-L. Kim, “Communication-Efficient On-Device Machine Learning: Federated Distillation and Augmentation under Non-IID Private Data,” 2023. [Online]. Available: https://arxiv.org/abs/1811.11479

[29] Z. Wang, Y. Zhou, Y. Shi, and Khaled. B. Letaief, “Federated Low-Rank Adaptation for Large Language Model Fine-Tuning Over Wireless Networks,” in *GLOBECOM 2024 - 2024 IEEE Global Communications Conference*, 2024, pp. 3063–3068. doi: 10.1109/GLOBECOM52923.2024.10901572.

[30] Z. Gao, Z. Zhang, Y. Guo, and Y. Gong, “Federated Adaptive Fine-Tuning of Large Language Models with Heterogeneous Quantization and LoRA,” in *IEEE INFOCOM 2025 - IEEE Conference on Computer Communications*, 2025, pp. 1–10. doi: 10.1109/INFOCOM55648.2025.11044641.

[31] Z. Sasindran, H. Yelchuri, and T. V Prabhakar, “Ed-Fed: A generic federated learning framework with resource-aware client selection for edge devices,” in *2023 International Joint Conference on Neural Networks (IJCNN)*, 2023, pp. 1–8. doi: 10.1109/IJCNN54540.2023.10191316.

[32] H. Wang *et al.*, “ROFED-LLM: Robust Federated Learning for Large Language Models in Adversarial Wireless Environments,” *IEEE Trans. Netw. Sci. Eng.*, pp. 1–13, 2025, doi: 10.1109/TNSE.2025.3590975.

[33] Y. Lin, S. Han, H. Mao, Y. Wang, and W. J. Dally, “Deep Gradient Compression: Reducing the Communication Bandwidth for Distributed Training,” 2020. [Online]. Available: https://arxiv.org/abs/1712.01887

[34] A. F. Aji and K. Heafield, “Sparse Communication for Distributed Gradient Descent,” Association for Computational Linguistics, Sep. 2017, pp. 440–445. doi: 10.18653/v1/D17-1045.

[35] Y. Shen *et al.*, “Large Language Models Empowered Autonomous Edge AI for Connected Intelligence,” *IEEE Communications Magazine*, vol. 62, no. 10, pp. 140–146, 2024, doi: 10.1109/MCOM.001.2300550.

[36] H. B. McMahan, D. Ramage, K. Talwar, and L. Zhang, “Learning Differentially Private Recurrent Language Models,” 2018. [Online]. Available: https://arxiv.org/abs/1710.06963

[37] Y. Jiang *et al.*, “Blockchained Federated Learning for Internet of Things: A Comprehensive Survey,” *ACM Comput. Surv.*, vol. 56, no. 10, Jun. 2024, doi: 10.1145/3659099.

[38] F. Lai, Y. Dai, X. Zhu, H. V Madhyastha, and M. Chowdhury, “FedScale: Benchmarking Model and System Performance of Federated Learning,” in *Proceedings of the First Workshop on Systems Challenges in Reliable and Secure Federated Learning*, New York, NY, USA: Association for Computing Machinery, 2021, pp. 1–3. doi: 10.1145/3477114.3488760.

[39] H. Zhao, W. Du, F. Li, P. Li, and G. Liu, “FedPrompt: Communication-Efficient and Privacy-Preserving Prompt Tuning in Federated Learning,” in *ICASSP 2023 - 2023 IEEE International Conference on Acoustics, Speech and Signal Processing (ICASSP)*, 2023, pp. 1–5. doi: 10.1109/ICASSP49357.2023.10095356.

[40] B.-L. Nguyen, T. C. Cao, and B. Le, “Meta-learning and Personalization Layer in Federated Learning,” in *Intelligent Information and Database Systems. ACIIDS 2022*, vol. 13757, N. T. Nguyen, T. K. Tran, U. Tukayev, T. P. Hong, B. Trawiński, and E. Szczerbicki, Eds., in Lecture Notes in Computer Science, vol. 13757. , Springer, Cham, 2022, pp. 209–221. doi: 10.1007/978-3-031-21743-2_17.

[41] L. Zhang, B. Tang, and J. Xu, “Lightweight verifiable privacy preserving federated learning,” *Journal of Network and Computer Applications*, vol. 244, p. 104335, 2025, doi: 10.1016/j.jnca.2025.104335.

[42] Z. Wang, B. Yan, and A. Dong, “Blockchain Empowered Federated Learning for Data Sharing Incentive Mechanism,” *Procedia Comput. Sci.*, vol. 202, pp. 348–353, 2022, doi: 10.1016/j.procs.2022.04.047.

[43] Y. Cheng, W. Zhang, Z. Zhang, C. Zhang, S. Wang, and S. Mao, “Toward Federated Large Language Models: Motivations, Methods, and Future

Directions," *IEEE Communications Surveys & Tutorials*, vol. 27, no. 4, pp. 2733–2764, 2025, doi: 10.1109/COMST.2024.3503680.

[44] G. Guan, T. Zhi, H. Cai, Y. Cao, and H. Xie, "Hierarchical Federated Learning Privacy Protection Framework with Enhanced Privacy and Resistance to Byzantine Attacks," in *2024 IEEE 7th International Conference on Computer and Communication Engineering Technology (CCET)*, 2024, pp. 250–256. doi: 10.1109/CCET62233.2024.10838122.

[45] X. L. Li and P. Liang, "Prefix-Tuning: Optimizing Continuous Prompts for Generation," in *Proceedings of the 59th Annual Meeting of the Association for Computational Linguistics and the 11th International Joint Conference on Natural Language Processing (Volume 1: Long Papers)*, C. Zong, F. Xia, W. Li, and R. Navigli, Eds., Online: Association for Computational Linguistics, Aug. 2021, pp. 4582–4597. doi: 10.18653/v1/2021.acl-long.353.

[46] Z. Ju, T. Wei, and F. Shen, "BEFL: Balancing Energy Consumption in Federated Learning for Mobile Edge IoT," 2024. [Online]. Available: https://arxiv.org/abs/2412.03950

[47] R. da Silva, O. L. A. López, and R. D. Souza, "Energy-Aware Federated Learning With Distributed User Sampling and Multichannel ALOHA," *IEEE Communications Letters*, vol. 27, no. 10, pp. 2867–2871, 2023, doi: 10.1109/LCOMM.2023.3312793.

[48] R. Ye, J. Chai, X. Liu, Y. Yang, Y. Wang, and S. Chen, "Emerging Safety Attack and Defense in Federated Instruction Tuning of Large Language Models," 2024. [Online]. Available: https://arxiv.org/abs/2406.10630

[49] B. Farahani, S. Tabibian, and H. Ebrahimi, "Toward a Personalized Clustered Federated Learning: A Speech Recognition Case Study," *IEEE Internet Things J.*, vol. 10, no. 21, pp. 18553–18562, 2023, doi: 10.1109/JIOT.2023.3292797.

# Chapter 3

## Mechanical Strength and Wear Behavior of Zinc–Aluminum Alloys Produced by Casting

**İhsan KIRIK**[1]

### 1. INTRODUCTION

In recent years, the search for high-performance yet low-cost materials in industrial design and manufacturing processes have significantly increased interest in zinc-aluminum (ZA) alloys. Copper-based bronze and cast irons, traditionally used as bearing materials and structural components, are increasingly being replaced by ZA alloys due to high raw material costs and production difficulties. Pioneering studies by Murphy et al. have defined the physical metallurgy of ZA alloys (especially ZA-8, ZA-12, and ZA-27), establishing a scientific basis for these materials to possess mechanical properties comparable to cast iron and bronze [1-8].

Since their creation as substitutes for bronze and cast iron, zinc-aluminum (ZA) casting alloys—a substantial family of non-ferrous alloys have drawn a lot of interest in industrial applications. These alloys, which usually have an aluminum content of 8–27 weight percent, are distinguished by their high strength, superior bearing qualities, strong resistance to corrosion, and ease of production using traditional casting methods [9-12].

The fundamental element determining the mechanical behavior of ZA alloys is the microstructural morphology formed after casting. With increasing aluminum content, the microstructure takes on a more complex dendritic structure. Research conducted by Savaşkan et al. has detailed how the ratios of aluminum and copper in the alloy alter the phase distribution in the microstructure and how this change affects the correlation between hardness and tensile strength. In the literature, the tensile strength of ZA-27, reaching levels of 450 MPa depending on its casting parameters, offers a strategic advantage for automotive components where a high strength-to-weight ratio is desired [13-14].

From a tribological perspective, ZA alloys exhibit superior performance, especially in conditions where lubrication is limited. Savaşkan's studies on wear mechanisms have confirmed that the oxide layer formed on the surface during

[1] Prof. Dr., Bingöl University, Bingöl Technical Sciences Vocational School / Machinery and Metal Technologies, Turkey, alihsankirik@gmail.com, (ORCID: 0000-0002-8361-319X)

friction by these zinc-based alloys minimizes adhesive wear, thus enabling them to exhibit lower wear rates than conventional SAE 660 bronze. However, the low melting temperatures and creep susceptibility of these alloys remain a fundamental limitation in high-temperature applications. It is the main alloying element that gives fluidity to aluminum-Zn alloys [9-17]. In practice, the amount of Al added to Zn-based alloys varies widely to achieve good engineering properties. In addition, small amounts of copper and magnesium are added to obtain the best combination in terms of mechanical properties and castability. Research on ZA alloys has been further spurred by the growing need for lightweight, high-performance, and economical materials. The composition of the alloy, the casting process, and the subsequent microstructural development all have a significant impact on their mechanical and tribological characteristics. Therefore, improving ZA alloys for advanced engineering applications requires an understanding of the link between manufacturing factors, microstructure, and performance [18-21].

Zinc-based alloys have been widely used in engineering applications due to their excellent castability, good corrosion resistance, and relatively low production cost. Among these materials, zinc–aluminum (Zn–Al) alloys have attracted considerable attention because of their superior mechanical and tribological properties compared to pure zinc, making them suitable for bearings, bushings, gears, and other wear-resistant components used in automotive and industrial applications [41].

The mechanical and functional properties of Zn–Al alloys are strongly influenced by aluminum content. Abou El-Khair (2004) demonstrated that increasing the aluminum content in Zn–Al binary alloys significantly enhance hardness, tensile strength, and wear resistance, although this improvement is accompanied by a reduction in ductility. The same study also revealed that increasing temperature leads to a decrease in strength and an increase in ductility, while higher aluminum contents provide improved strength retention at elevated temperatures. These findings highlight the importance of alloy design in extending the service performance of Zn–Al alloys under thermal exposure [13].

Beyond aluminum, alloying with secondary elements has been widely explored to further improve the mechanical and tribological performance of Zn–Al alloys. Türk et al. (2007) investigated the wear behavior of a commercial ZA-8 alloy modified with Pb, Sn, and Cd, and compared its performance with SAE 660 bearing bronze. Their results indicated that both unmodified and modified ZA alloys exhibit superior wear resistance compared to bearing bronze, although they also show a higher coefficient of friction [36]. Similarly, Savaşkan et al. (2014) examined the effects of copper and silicon additions in Zn–Al alloys with

a constant aluminum content of 15 wt.% [34]. They reported that copper additions significantly increase hardness, tensile strength, and compressive strength, while elongation and impact energy decrease. For Zn–Al–Cu–Si alloys, increasing silicon content improved hardness and compressive strength but adversely affected tensile properties and ductility.

Magnesium has been widely recognized as an effective alloying element in aluminum- and magnesium-based alloy systems due to its contribution to solid-solution strengthening, precipitation hardening, and microstructural refinement [41]. In Al–Mg and Al–Si–Mg alloys, Mg-containing intermetallic phases have been shown to improve wear resistance and enhance mechanical stability at elevated temperatures [44]. Although studies focusing on magnesium additions in Zn–Al alloys are relatively limited, available research suggests that Mg promotes grain refinement and modifies the solidification behavior, leading to increased hardness and strength through the formation of fine intermetallic compounds [42, 43]. However, excessive Mg additions may result in brittle phase formation, which can negatively affect ductility and impact resistance.

Wear resistance is one of the most critical functional performance criteria for Zn–Al alloys, particularly for sliding and bearing applications. Previous studies have reported a strong correlation between hardness and wear resistance in Zn–Al and Zn–Al–Cu alloys, while the dominant wear mechanisms are strongly dependent on alloy composition and operating conditions [16, 50]. In addition, Zn–Al alloys are known to suffer from thermal softening and microstructural coarsening at elevated temperatures, which limits their high-temperature performance [2, 6]. Alloying additions such as Cu, Si, and Mg have therefore been investigated as potential approaches to enhance thermal stability and resistance to high-temperature deformation [26, 44].

Despite the extensive body of literature on Zn–Al-based alloys, the combined effects of systematic magnesium additions and post-casting heat treatment on the microstructural evolution, mechanical properties, and functional performance of ZA alloys have not been comprehensively addressed. Most existing studies focus on individual alloying elements or room-temperature mechanical behavior, leaving a gap in understanding the synergistic influence of Mg content and heat treatment on wear resistance and thermal stability [22-27].

Therefore, the novelty of the present study lies in the integrated investigation of magnesium-alloyed ZA alloys produced by casting and subjected to controlled heat treatment conditions. The primary objectives are to clarify the role of Mg addition on phase formation and microstructural refinement, to quantify its effects on hardness and mechanical performance, and to evaluate the functional properties of the alloys in terms of wear behavior and high-temperature stability.

The findings aim to establish clear structure–property relationships and to contribute to the development of high-performance Zn–Al–Mg alloys for advanced engineering applications. Moreover, mechanical strength and wear behavior of different ZA alloys produced by casting, considering the fundamental principles introduced to the literature by other researchers and will analyze the effects of aluminum variations on hardness and discuss the wear modes (adhesive, abrasive, and oxidative) exhibited by the material under different loading conditions using microscopic methods [28-34].

Because of their superior castability, high strength-to-weight ratio, good wear resistance, and affordability as compared to conventional bronze and cast-iron components, zinc-aluminum (ZA) casting alloys are frequently used engineering materials. The production processes of ZA casting alloys are reviewed and discussed in this article, with an emphasis on their microstructural features and the ensuing mechanical and tribological properties. A critical analysis is conducted of the connections between alloy composition, solidification behavior, microstructure evolution, hardness, strength, and wear performance. Emphasis is placed on commonly used ZA alloys such as ZA-8, ZA-12, and ZA-27, highlighting their suitability for bearing, bushing, and automotive applications

## 2. PRODUCTION OF ZA CASTING ALLOYS

### 2.1 Alloy Composition and Classification

ZA casting alloys are commonly classified based on their aluminum content. Al content exerts a dominant influence on phase equilibria, solidification pathways, and the evolution of microstructural constituents, thereby controlling the mechanical and tribological performance of the alloys. The principal commercial grades include ZA-8, ZA-12, and ZA-27, containing nominally 8, 12, and 27 wt.% Al, respectively [9,14]. An increase in aluminum content enhances the volume fraction of α-Al–rich phases and promotes eutectoid transformation within the Zn–Al system, resulting in progressive improvements in hardness, yield strength, and wear resistance, accompanied by a reduction in ductility and fracture toughness [22]. Accordingly, ZA-8 alloys exhibit superior fluidity and elongation, making them suitable for thin-walled and dimensionally complex die-cast components, whereas ZA-12 alloys provide an optimized compromise between castability and load-bearing capacity for automotive and general engineering applications. In contrast, ZA-27 alloys demonstrate markedly higher strength and creep resistance but increased susceptibility to hot cracking and microstructural coarsening, restricting their application primarily to bearing materials and heavily loaded structural components where replacement of copper-based alloys or cast iron is desired [38, 51]. Examples of parts produced

using the casting method of ZA alloys for different machine parts are given in Figure 1.

**Figure 1.** Parts produced using the casting method of ZA alloys for different machine parts.

### 2.2. Melting and Casting Techniques

Because of the low melting temperature of zinc (419°C), high vapor pressure, and severe oxidation propensity of aluminum, the melting and casting of zinc–aluminum (ZA) alloys necessitate stringent control of temperature, alloy chemistry, and furnace environment. Zinc evaporation, aluminum oxidation, gas porosity, segregation, and degradation of mechanical and tribological properties can all be caused by inadequate process control [37,51]. Tables 1 and 2, respectively, show the melting conditions and casting technique.

**Table 1.** Typical melting and processing parameters for ZA casting alloys

| Alloy | Al content (wt.%) | Melting temperature (°C) | Pouring / injection temperature (°C) | Recommended furnace type | Atmosphere control |
|---|---|---|---|---|---|
| ZA-8 | ~8 | 480–520 | 500–540 | Resistance / Induction | $N_2$ / Ar + flux |
| ZA-12 | ~12 | 500–550 | 520–570 | Resistance / Induction | $N_2$ / Ar + flux |
| ZA-27 | ~27 | 550–600 | 580–620 | Induction / Gas crucible | $N_2$ / Ar + flux |

**Table 2.** Comparison of casting techniques for ZA alloys

| Casting technique | Suitable alloys | Cooling rate | Surface quality | Mechanical properties | Production rate | Typical applications |
|---|---|---|---|---|---|---|
| **Hot chambers die casting** | ZA-8, ZA-12 | Very high | Excellent | High | Very high | Precision parts, automotive fittings |
| **Cold chambers die casting** | ZA-12, ZA-27 | High | Very good | Very high | High | Bearings, structural components |
| **Permanent mold casting** | All grades | Medium | Good | Medium–high | Medium | Engineering components |
| **Sand casting** | All grades | Low | Moderate | Medium | Low | Large parts, prototypes |

### 2.2.1. Melting Practice

ZA alloys are frequently melted in gas-fired crucible furnaces, electric resistance furnaces, or induction furnaces. Depending on the alloy quality and amount of aluminum, melting temperatures typically range from 480 to 600 °C. Greater superheating is necessary for alloys with greater aluminum concentrations, such as ZA-27, to guarantee full dissolution of alloying elements and chemical homogeneity [14].

During melting, several safeguards are put in place to reduce oxidation and compositional losses. Fluxes based on chloride and fluoride are frequently used to dissolve surface oxides and prevent the production of dross. Nitrogen or argon inert gas shielding is commonly used to lower hydrogen absorption and zinc evaporation. Degassing treatments are used to reduce dissolved gas concentration and stop porosity formation in cast products. These treatments are typically carried out by argon or nitrogen bubbling [51]. To minimize oxidation losses and

preserve exact compositional control, alloying elements like copper and magnesium are usually added after zinc has completely melted. Melt chemistry must be continuously monitored, especially for high performance bearing grades.

### 2.2.2. Casting Techniques

- **Hot-Chamber Die Casting**

Because of their exceptional fluidity and limited solidification range, ZA alloys can be processed using a variety of casting techniques. The most common industrial process for ZA-8 and ZA-12 alloys is hot-chamber die casting. This method (see in picture 2) involves injecting molten metal straight into the die cavity from an integrated furnace chamber. Benefits consist of efficiency in production, minimal post-processing needs, tight dimensional tolerances and superior surface finish. However, because aluminum dissolution causes severe corrosion of submerged components, this approach is inappropriate for high-aluminum alloys as ZA-27 [9,14].

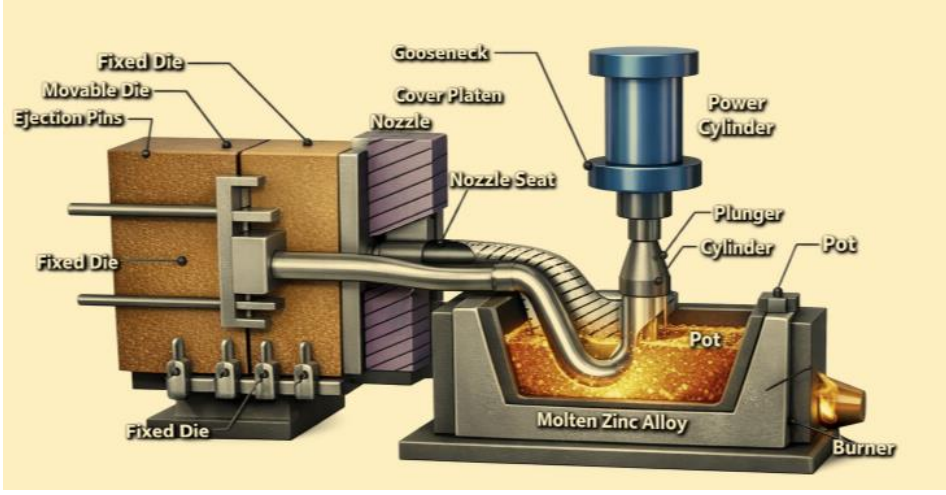


**Figure 2**. Hot-Chamber Die Casting method [52].

- **Cold-Chamber Die Casting**

Because of their higher melting temperatures and greater chemical aggression toward steel-based injection components, cold-chamber die casting is the preferred manufacturing method for ZA alloys with aluminum contents greater than about 15 weight percent, especially for high-aluminum grades like ZA-27. The physical separation of the melting furnace from the injection unit, as opposed to hot-chamber systems, greatly minimizes corrosion, erosion, and aluminum dissolving of submerged mechanical parts. Using a ladle, the molten ZA alloy is

moved from the holding furnace into the shot sleeve. The melt is then forced into the closed die chamber at high pressure and velocity by a hydraulically operated plunger (see in picture 3). For ZA-27 alloys, typical injection pressures fall between 20 and 70 MPa, and melt temperatures are kept between 580 and 620 °C to guarantee sufficient fluidity and full mold filling. Wider process windows and higher superheating levels are two of cold chamber die casting's main benefits. This allows for better alloy homogeneity and a lower chance of premature solidification during injection. Tensile strength, hardness, and wear resistance are all improved by the controlled precipitation of ε intermetallic phases and the development of refined η + α microstructures, which are facilitated by the high cooling rates attained during mold filling [13-16].

But the approach has certain drawbacks as well. The possibility of melt contamination, temperature swings, and oxide entrainment is increased by the human or automated ladling process, which could negatively impact surface smoothness and result in the creation of gas porosity. Additionally, compared to hot chamber die casting, cycle times are typically higher, which results in a lower production efficiency. Despite these disadvantages, cold-chamber die casting is still the most popular method for producing high-performance ZA-27 parts for load-bearing applications, including tribological elements, bearings, bushings, and structural brackets. Die cast components with intricate shapes, delicate surface details, and thick or thin wall portions can all be used with this method.

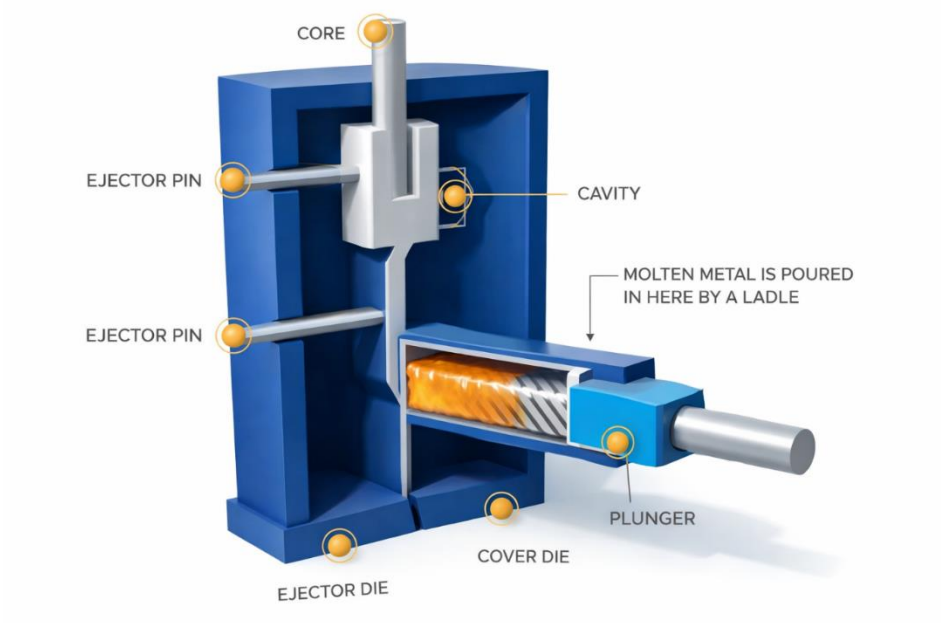


**Figure 3**. Cold-Chamber Die Casting method [47].

- **Sand Casting and Gravity**

For large components or low-volume production, gravity and sand-casting techniques are used. These methods result in coarser η + α microstructures and greater segregation due to comparatively slow cooling rates, which lower mechanical strength in comparison to die-cast counterparts. However, they are still appropriate for manufacturing prototypes and thick-section structural components [13-16].

- **Casting with a permanent mold**

Permanent mold casting offers better cooling control, finer microstructures, and reasonable tooling costs, making it a middle ground between sand casting and die casting. This process is very useful for producing technical components in medium quantities**.**

## 3. COMMON DIE CASTING ALLOYS

### 3.1. Zinc Alloys:

Due to its advantageous combination of castability, mechanical strength, wear resistance, and cost effectiveness, ZA (zinc–aluminum) alloys have been thoroughly studied as high-performance engineering materials for die casting applications. According to early fundamental research, adding more aluminum to

zinc-based alloys dramatically changes their phase structure and mechanical response, improving hardness and tensile strength while somewhat decreasing ductility [12,16]. The distribution of the η (Zn-rich) and α (Al-rich) phases, along with ε-type intermetallic compounds that become prominent in high-aluminum grades like ZA-27, are the main factors influencing the properties of ZA alloys, according to subsequent microstructural investigations [18,33]. Studies on heat treatment also showed that solution treatments and controlled aging can alter phase morphology and precipitate distribution, improving dimensional stability and strength-ductility balance [18].

One of the aspects of ZA alloys that has been studied the most is tribological performance. ZA alloys have been shown in numerous experiments to have better wear resistance than traditional bronze bearing, especially in dry sliding situations [32,36]. By encouraging the creation of fine intermetallic dispersions and fortifying the α phase matrix, the addition of copper and silicon has been demonstrated to further improve wear resistance and impact toughness. ZA alloys are now more suitable for heavy-duty tribological applications because of reinforcement with ceramic particles like SiC, which has been shown to dramatically increase hardness and lower friction coefficients. All things considered, the literature unequivocally shows that ZA alloys hold a special place between conventional zinc alloys and aluminum bronzes, providing an alluring combination of castability, mechanical strength, and tribological performance. To increase the usage of ZA alloys in high-load structural, automotive, and precision mechanical applications, current research trends increasingly focus on microstructure control, alloying techniques, and improved process optimization [21,22,35].

### 3.2. Aluminum Alloys:

Aluminum alloys remain the dominant materials in high-pressure die casting applications due to their favorable combination of mechanical strength, low density, and high thermal conductivity, which enable the production of lightweight structural components with efficient heat dissipation. Typical aluminum die casting alloys exhibit densities of approximately 2.7 $g \cdot cm^{-3}$ and are therefore particularly attractive for automotive and aerospace components where weight reduction is a critical design criterion [5,6]. In contrast, ZA (Zn–Al) alloys possess higher densities (≈5.0–6.0 $g \cdot cm^{-3}$) but offer superior castability, lower melting temperatures, and exceptional dimensional accuracy, making them highly suitable for precision components with complex geometries and tight tolerances [1,8]. Consequently, aluminum alloys dominate lightweight structural casting markets, while ZA alloys occupy a complementary niche in

high-precision, load bearing, and wear-critical components where dimensional stability and tribological performance are of primary importance [1].

### 3.3. Magnesium Alloys:

Magnesium alloys are prized for their high strength and incredibly low density. They are being investigated more for cutting-edge automotive applications where reducing weight immediately increases energy efficiency [26-28]. The advancements and prospects for HPDC magnesium alloys in the transportation industry are covered in recent synthesized review publications.

### 3.4. Copper Alloys:

Due to the inherently high electron mobility of copper-rich matrices, copper-based alloys are mostly used in applications where high electrical and thermal conductivity is crucial, such as electrical connectors, busbars, switching components, and heat exchanger systems. In high-purity compositions, these alloys usually have thermal conductivities greater than 300 $W \cdot m^{-1} \cdot K^{-1}$ and electrical conductivities close to 90–100% IACS, which far outperform casting alloys based on aluminum and zinc in terms of heat and current transport efficiency. Copper-based alloys are still useful for specific applications that need a combination of high conductivity, moderate mechanical strength, and corrosion resistance, even though their use in die casting is relatively restricted due to their high melting temperatures, elevated oxidation tendency, and increased tool wear. Precision components like rotor bars, thermal management components, and high-load electrical contacts can be produced by effectively processing advanced copper alloys like brasses and bronzes using pressure-assisted casting processes [33-44].

### 3.5. Lead Alloys:

However, lead-based alloys can still be used judiciously in specialized applications that call for extraordinarily high density, efficient radiation shielding, or superior vibration dampening properties. Counterweights, ballast parts, acoustic damping components, and shielding structures for medical and nuclear equipment are typical examples. Lead-rich alloys have positive casting behavior from a metallurgical perspective due to their low melting temperature and great fluidity, but these benefits are typically overshadowed by their poor mechanical strength, limited fatigue resistance, and significant environmental effects. As a result, lead-based alloys are currently regarded as legacy materials in die casting technology and are only used in specific technical settings when other materials are unable to sufficiently meet functional requirements [11].

## 4. THE USE OF ALUMINUM IN DIE CASTING

Al alloys have excellent combination of low density, high specific strength, outstanding corrosion resistance, and attractive thermal properties, and are the most used material class in high-pressure die casting. Aluminum alloys, which have a density of about 2.7 $g \cdot cm^{-3}$, allow structural components to be significantly lighter. This is especially important in the automotive and aerospace industries, where lightweight design directly improves system performance, fuel efficiency, and emissions. From a metallurgical standpoint, Al–Si and Al–Si–Cu systems, which have superior fluidity, limited solidification ranges, and less vulnerability to hot ripping, are the main building blocks of aluminum die casting alloys. While copper and magnesium additives give precipitation strengthening and enhanced mechanical performance, silicon enhances castability and mold filling behavior. Tensile strength, fatigue resistance, and dimensional stability are all balanced in these alloys, which usually form an α-Al matrix reinforced by finely distributed eutectic silicon and intermetallic phases [1].

**Table 3.** Comparison of Aluminum, ZA (Zn–Al), and Copper Alloys for Die Casting Applications

| Property / Criterion | Aluminum Alloys (Al) | ZA Alloys (Zn–Al) | Copper Alloys (Cu) |
|---|---|---|---|
| Density ($g \cdot cm^{-3}$) | ~2.7 | ~5.0–6.0 | ~8.7–8.9 |
| Melting temperature (°C) | 580–660 | 380–490 | 900–1085 |
| Castability / Fluidity | Good | Excellent | Moderate–Poor |
| Dimensional accuracy | Good | Excellent | Moderate |
| Typical tensile strength (MPa) | 150–320 | 250–450 (ZA-27 up to ~480) | 200–400 |
| Specific strength | High | Moderate | Low |
| Wear resistance | Moderate | High | Moderate–High |
| Thermal conductivity ($W \cdot m^{-1} \cdot K^{-1}$) | 120–180 | 100–120 | 300–390 |
| Electrical conductivity (% IACS) | 35–60 | 25–30 | 80–100 |
| Corrosion resistance | Good | Good | Good–Excellent |
| Microstructural basis | α-Al + eutectic Si + precipitates | η (Zn-rich) + α (Al-rich) ± ε | α-Cu + intermetallics |
| Tool wear during casting | Moderate | Low | High |

| | | | |
|---|---|---|---|
| Cycle time in die casting | Moderate | Short | Long |
| Recyclability | Excellent | Excellent | Excellent |
| Typical applications | Automotive housing, aerospace parts, electronics | Bearings, gears, precision components, bushings | Electrical connectors, heat exchangers, rotor bars |
| Cost (relative) | Moderate | Low–Moderate | High |
| Environmental constraints | Low | Low | Low |

## 5. BENEFITS OF DIE CASTING MATERIALS

Die casting materials are ideal for high-volume production of intricate technical components because they provide a special blend of mechanical, physical, and financial benefits. These advantages result from both the inherent qualities of frequently used die casting alloys, like magnesium, zinc, and aluminum, and the features of the die casting process itself. The exceptional castability of die casting materials is one of their main benefits. Die casting alloys can produce thin-walled, geometrically complicated products with excellent dimensional precision because they usually have low melting temperatures, great fluidity, and good mold-filling capabilities. This is especially crucial for alloys based on zinc and aluminum, which are frequently used in high-pressure die casting (HPDC) applications.

Additionally, die casting materials offer excellent surface quality and dimensional stability. Die-cast components often require little post-processing because of their tight tolerances and flawless surface finish. As a result, there are fewer secondary machining operations, which lowers production costs and shortens manufacturing cycles. Particularly, zinc die casting alloys are renowned for their capacity to replicate minute details and preserve dimensional accuracy over extended service times. The advantageous strength-to-weight ratio that die casting alloys provide is another important advantage. For lightweight structural applications in the automotive and aerospace industries, aluminum and magnesium alloys are appealing due to their low density and comparatively high mechanical strength. Despite being denser, zinc-aluminum alloys offer greater stiffness and resistance to wear, which makes them appropriate for tribological and bearing components [6-22].

Another benefit of die casting materials, particularly alloys based on zinc and aluminum, is their good electrical and thermal conductivity. These characteristics make them suitable for use in thermal management components, heat sinks, and electronic housing. Furthermore, a lot of die casting alloys have strong corrosion

resistance, which can be improved by surface treatments or alloying additions [44]. Die casting materials offer high material efficiency and recyclability from an economic and sustainable standpoint. Alloys made of zinc and aluminum may be recycled repeatedly with little loss of quality, which lessens their impact on the environment and lowers the cost of raw materials. Die casting materials are also very affordable for mass production because to the long service life of die casting dies and the high production rates possible with HPDC techniques.

The benefits of die casting materials include excellent castability, high dimensional accuracy, favorable mechanical properties, good thermal performance, and economic efficiency. These advantages explain their widespread adoption across automotive, electronics, and consumer goods industries and justify the continued research and development efforts focused on optimizing die casting alloy compositions and processing parameters.

## 6. SOLIDIFICATION BEHAVIOR

Thermal history, cooling circumstances during casting, and chemical composition (especially the Al concentration) all have a significant impact on the solidification behavior of zinc-aluminum (ZA) alloys. In the Zn–Al binary system, commercial ZA grades like ZA-8, ZA-12, and ZA-27 exhibit hypoeutectic to near-eutectic compositions, where the alloy's position with respect to the eutectic point in the phase diagram determines the solid phase sequence and morphology.

Solidification usually starts with the nucleation and development of primary α-Al (Al-rich) dendrites from the molten alloy for hypoeutectic ZA alloys (low to moderate Al concentration). According to the equilibrium phase diagram for Zn–Al systems, a eutectic reaction takes place as the temperature drops near the eutectic point, resulting in a fine mixture of α-Al and η (Zn-rich) phases in the remaining liquid. This results in a final microstructure whose shape depends on both composition and cooling rate, and which consists of primary α dendrites embedded in an interdendritic, lamellar α + η eutectic matrix. While slower cooling produces coarser structures and phase segregation, rapid cooling tends to refine dendritic arm spacing and eutectic characteristics. Higher cooling rates limit solute redistribution and secondary phase formation, promoting finer microstructural features and improving mechanical qualities including strength and hardness, according to experimental research [44-47].

## 7. MICROSTRUCTURAL CHARACTERISTICS

Depending on composition and cooling conditions, the microstructure of ZA casting alloys usually consists of several intermetallic compounds, an aluminum-rich α phase, and a zinc-rich η phase. Higher aluminum alloys, like ZA-27, have coarser dendritic structures, while low-aluminum alloys, like ZA-8, have more fine and uniform microstructures. Cu-rich intermetallic, which increase hardness and strength but can decrease ductility if present in excess, are frequently found in copper-containing ZA alloys. The overall mechanical and tribological behavior of the alloy is largely determined by the distribution, size, and shape of these phases.

**Table 4.** Typical Microstructural Characteristics by Grade of Alloy

| Alloy | Al content (wt%) | Microstructural Features | Properties |
|---|---|---|---|
| ZA-8 | 7–8 | α-Zn matrix, fine eutectic, few intermetallic | High ductility, moderate strength |
| ZA-12 | 12 | α-Zn dendrites, β-Zn–Al intermetallic plates, eutectic at boundaries | Balanced strength and ductility |
| ZA-27 | 27 | Coarse β and η intermetallic, α-Zn matrix reduced | High hardness and strength, lower ductility |

## 8. HARDNESS, MECHANICAL STRENGTH, WEAR PROPERTIES AND TRIBOLOGICAL BEHAVIOR

The hardness of ZA alloys increases with aluminum and copper content due to the formation of hard intermetallic phases and solid solution strengthening. ZA-27 typically exhibits the highest hardness among common ZA alloys, making it suitable for applications requiring high surface durability and wear resistance. Heat treatment and aging can further modify hardness by promoting phase transformations and precipitation processes. However, excessive aging may lead to dimensional instability, which must be carefully controlled in precision components. ZA alloys demonstrate high tensile and compressive strength compared to traditional zinc alloys. The strength generally increases with aluminum content, while ductility decreases. Fine-grained microstructures obtained through controlled casting conditions are beneficial for achieving an optimal balance between strength and toughness [35,36].

The load-bearing capability of ZA alloys makes them particularly attractive for structural and bearing applications, where resistance to deformation under high stress is critical. The wear resistance of ZA casting alloys is one of their most important attributes. Their excellent performance under sliding conditions is attributed to a combination of high hardness, the presence of lubricating zinc-rich

phases, and the ability to form stable tribolayers during wear. ZA alloys generally exhibit lower wear rates than aluminum alloys and comparable performance to bronze in dry and lubricated conditions. The wear mechanism is typically a combination of adhesive and mild abrasive wear, with the dominant mechanism depending on load, sliding speed, and counter face material. Higher aluminum and copper contents improve wear resistance but may increase friction coefficients. Therefore, alloy selection must consider the specific operating conditions of the intended application[37,38].

## 9. CONCLUSIONS

With an emphasis on the impact of alloy composition and microstructure, this study examined the mechanical strength and wear behavior of zinc-aluminum (ZA) alloys made via casting. The following is a summary of the main conclusions:

1. Microstructural Influence: It was discovered that the zinc-to-aluminum ratio has a significant impact on the microstructure of ZA alloys. A finer dendritic structure was encouraged by a higher aluminum concentration, which enhanced wear resistance and hardness.
2. Mechanical Properties: ZA alloys have good mechanical strength, as shown by tensile and compressive testing. Certain compositions provide the best balance between ductility and hardness. Alloy design is essential for customizing mechanical performance, as seen by the strong correlation between hardness tests and microstructural refinement.
3. Wear Behavior: ZA alloys with a homogeneous microstructure and greater hardness showed better frictional behavior and reduced wear rates, according to wear testing. The consistent distribution of secondary phases inside the matrix lessened the severity of the wear mechanisms, which were mainly sticky and abrasive.
4. Practical Implications: ZA alloys are appropriate for use in automotive, industrial, and mechanical components where durability under sliding or frictional contact is necessary because of their high strength, hardness, and wear resistance.
5. Future Work: To improve the tribological and mechanical performance of ZA alloys for high-demand applications, more investigation into sophisticated casting methods, heat treatments, and alloying additions is advised.
6. Overall, the study shows that the mechanical and wear characteristics of ZA alloys may be optimized by careful control of alloy composition and

casting parameters, offering an affordable substitute for traditional engineering metals.

7. Zinc-aluminum (ZA) casting alloys are ideal for a variety of engineering applications due to their special blend of high strength, outstanding hardness, and exceptional wear resistance. Alloy composition, casting technique, and the resulting microstructure all have a significant impact on the mechanical, tribological, and thermal properties of these alloys, underscoring the crucial role that processing circumstances play in determining performance.
8. For ZA alloys to be designed and optimized effectively, a thorough understanding of the connections between production parameters, microstructure, and characteristics is necessary. It is anticipated that developments in surface engineering, heat treatment, controlled solidification, and microstructural refinement will improve their performance and increase the range of possible applications. To satisfy the increasing demand for high-performance engineering components, future research should also concentrate on innovative alloy compositions and additive manufacturing techniques.

**REFERENCES**


1. ASM International. (2018a). *ASM handbook, Volume 2: Properties and selection – Nonferrous alloys and special-purpose materials*. ASM International.
2. ASM International. (2018b). *ASM handbook, Volume 15: Casting*. ASM International.
3. Callister, W. D., & Rethwisch, D. G. (2020). *Materials science and engineering: An introduction* (10th ed.). Wiley.
4. Campbell, J. (2015). *Complete casting handbook: Metal casting processes, metallurgy, techniques and design* (2nd ed.). Butterworth-Heinemann.
5. Davis, J. R. (Ed.). (2001). *Copper and copper alloys*. ASM International.
6. Davis, J. R. (Ed.). (2004). *Aluminum and aluminum alloys*. ASM International.
7. Kaufman, J. G., & Rooy, E. L. (2004). *Aluminum alloy castings: Properties, processes, and applications*. ASM International.
8. Polmear, I. J. (2006). *Light alloys: From traditional alloys to nanocrystals* (4th ed.). Elsevier Butterworth-Heinemann.
9. Totten, G. E., & MacKenzie, D. S. (2003). *Handbook of aluminum: Volume 2 – Alloy production and materials manufacturing* (2nd ed.). CRC Press.
10. Çöpcü, M. (2002). *Extractive metallurgy of copper*. W. G. Davenport; M. J. King; M. E. Schlesinger.
11. Schlesinger, M. E. (2014). *Extractive metallurgy of copper* (5th ed.). Elsevier.
12. Abou El-Khair, M. T., Daoud, A., & Ismail, A. (2004). Effect of different Al contents on the microstructure, tensile and wear properties of Zn-based alloy. *Materials Letters, 58*(11), 1754–1760. https://doi.org/10.1016/j.matlet.2003.10.05
13. Abou El-Khair, M. Y. (2004). Effect of aluminum content on the mechanical properties of Zn–Al alloys. *Journal of Materials Science, 39*(3), 1001–1008. https://doi.org/10.1023/B:JMSC.0000012946.92145.3f
14. Agarwal, A., & Dahotre, N. B. (2020). Phase transformations and mechanical properties in Zn–Al based casting alloys. *Journal of Materials Engineering and Performance, 29*(4), 2035–2047. https://doi.org/10.1007/s11665-020-04893-x
15. Alesdair, S., & Murphy, S. (1991). Structure and properties of ternary Zn–Al–Cu alloys. *Materials Science and Technology, 7*(12), 1101–1109.
16. Murphy, S. (1982). The physical metallurgy of zinc–aluminum alloys. *Journal of Metals, 34*(3), 27–32.

17. Sabet, M., et al. (2021). Microstructure and mechanical properties of ZA alloys: A review. *Journal of Materials Research and Technology, 15*, 3495–3510. https://doi.org/10.1016/j.jmrt.2021.06.012
18. Yildiz, F., Savaşkan, M. E., & Murphy, S. (2009). Effect of heat treatment on microstructure and mechanical properties of ZA alloys. *Materials Characterization, 60*(9), 1013–1018. https://doi.org/10.1016/j.matchar.2009.04.009
19. Zhao, Y., Fu, Q., & Li, D. (2023). Solidification pathways, phase equilibria, and mechanical behavior of Zn–Al casting alloys with emphasis on ZA-27. *Journal of Alloys and Compounds, 939*, 168585.
20. Babic, M., Mitrovic, S., & Ninkovic, R. (2010). Tribological behaviour of zinc–aluminium alloys under dry sliding conditions. *Tribology International, 43*, 125–134.
21. Babic, M., Rac, A., & Stojanovic, B. (2010). Tribological behavior of zinc–aluminum alloys. *Tribology in Industry, 32*(2), 3–11.
22. Babic, M., Mitrovic, S., Ninkovic, R., & Dzunic, D. (2013). Tribological behavior of ZA alloys reinforced with SiC particles. *Tribology International, 63*, 54–62. https://doi.org/10.1016/j.triboint.2012.01.012
23. Çuvalcı, H., & Bas, H. (2004). Investigation of the tribological properties of silicon containing zinc–aluminum based journal bearings. *Tribology International, 37*, 433–440.
24. Çuvalcı, H., & Çelik, H. S. (2011). Investigation of the abrasive wear behaviour of ZA-27 alloy and CuSn10 bronze. *Journal of Materials Science, 46*, 4850–4857.
25. Li, Y., Ngai, T. L., Xia, W., & Zhang, W. (1996). Effects of Mn content on the tribological behaviors of Zn-27%Al-2%Cu alloy. *Wear, 198*, 129–135.
26. Miroslav, B., Vencl, A., Mitrović, S., & Bobić, I. (2009). Influence of T4 heat treatment on tribological behavior of ZA-27 alloy. *Tribology Letters, 36*, 125–134.
27. Miroslav, B., Mitrović, S., Zivic, F., & Bobić, I. (2010). Wear behavior of composites based on ZA-27 alloy reinforced by $Al_2O_3$ particles. *Tribology Letters, 38*, 337–346.
28. Mondal, D. P., Das, S., & Jha, A. K. (2004). Dry sliding wear behaviour of zinc–aluminium alloys. *Wear, 256*, 794–804.
29. Pola, A., Tocci, M., & La Vecchia, G. M. (2012). Zinc alloys for casting: Mechanical and tribological properties. *Journal of Materials Processing Technology, 212*, 264–273.
30. Prasad, B. K., & Yegneswaran, A. H. (1997). Dry sliding wear behaviour of zinc-based alloys. *Wear, 203–204*, 316–327.

31. Prasad, B. K., Patwardhan, A. K., & Yegneswaran, A. H. (1997). Dry sliding wear characteristics of zinc-based alloys: Influence of aluminum content. *Zeitschrift für Metallkunde, 88*(4), 333–338.
32. Savaşkan, T., & Laufer, E. E. (1986). Wear resistance of cast zinc–aluminum alloys. *Wear, 112*(3–4), 267–276.
33. Savaşkan, T., & Murphy, S. (1987). Mechanical properties and lubricated wear of Zn-25Al-based alloys. *Wear, 116*(2), 211–224. https://doi.org/10.1016/0043-1648(87)90234-1
34. Savaşkan, T., & Purcek, G. (2002). Effect of copper content on the mechanical and tribological properties of Zn-27Al-based alloys. *Tribology International, 35*(6), 395–401.
35. Sharma, S. C., & Anand, A. (2006). Wear behaviour of zinc-based alloys reinforced with SiC particles. *Materials Science and Engineering: A, 417*, 178–188.
36. Türk, G., Savaşkan, M. E., & Küçükömeroğlu, T. (2007). Wear behavior of modified ZA-8 alloys. *Wear, 262*(11–12), 1407–1414. https://doi.org/10.1016/j.wear.2007.01.004
37. Zhu, S., & Song, G. (2017). Influence of alloying elements on wear and thermal stability of zinc-based alloys. *Wear, 376–377*, 1285–1293.
38. Kumar, S., Prasad, S. R., & Singh, A. (2022). Tribological performance and phase stability of high-aluminum ZA alloys. *Wear, 494–495*, 204315. https://doi.org/10.1016/j.wear.2021.204315
39. Anwar, M., & Murphy, S. (2000). Creep kinetics in compression of sand cast commercial Zn–Al alloys. *Materials Science and Technology, 16*, 321–332.
40. Wu, Z., Sandlöbes, S., Wang, Y., Gibson, J. S. K.-L., & Korte-Kerzel, S. (2018). Creep behaviour of eutectic Zn-Al-Cu-Mg alloys. *Materials Science and Engineering: A, 724*, 80–94.
41. Gervais, E., Levert, H., & Bess, M. (1980). Development of zinc-base foundry alloys. *Transactions of the American Foundrymen's Society, 68*, 183–194.
42. Haroan, G., & Jiaji, M. (1999). Alloying of Zn-27%Al with antimony. *International Journal of Cast Metals Research, 11*, 205–210.
43. Savaşkan, M. E., Aydiner, A., & Murphy, S. (2014). Effects of copper and silicon additions. *Journal of Alloys and Compounds, 586*, 705–712. https://doi.org/10.1016/j.jallcom.2013.10.079
44. Bakhsheshi-Rad, H. R., Idris, M. H., Kadir, M. R. A., & Farahany, S. (2012). Microstructure and corrosion behavior of biodegradable Zn–Al–

Mg alloys. *Materials Science and Engineering: C, 32*(8), 2456–2462. https://doi.org/10.1016/j.msec.2012.07.012

45. Zhang, E., Yin, D., Xu, L., Yang, L., & Yang, K. (2009). Microstructure and biocompatibility of Zn–Mg alloys. *Biomaterials, 30*(4), 713–721.
46. Jiang, P., Blawert, C., & Zheludkevich, M. L. (2020). Corrosion performance of Mg–Zn based alloys: A review. *Corrosion and Materials Degradation, 1*(1), 92–158. https://doi.org/10.3390/cmd1010007
47. Chavan, R., & Kulkarni, P. S. (2020). Cooling channel optimization in HPDC. *IOP Conference Series: Materials Science and Engineering, 810*(1), 012017. https://doi.org/10.1088/1757-899X/810/1/012017
48. Lehmhus, D. (2022). Advances in metal casting technology. *Metals, 12*(11), 1959.
49. Li, D., Slater, C., Cai, H., Hou, X., Li, Y., & Wang, Q. (2023). Joining technologies for aluminium castings. *Coatings, 13*(5), 958.
50. Yang, J., Liu, H., & Huang, H. (2023). Composition–process–property prediction of die casting Al alloys. *Journal of Materials Research and Technology, 28*, 335–346. https://doi.org/10.1016/j.jmrt.2023
51. Zhao, H.-D., Wang, X.-L., Wan, Q., Bai, W.-H., & Liu, F. (2024). High-pressure die cast alloys: A review. *China Foundry, 21*, 427–444.
52. https://www.sunrise-metal.com/what-is-hot-chamber-die-casting/

# Chapter 4

# Densification Kinetics and Property–Microstructure Investigations in Powder Metallurgy Cobalt Matrix Composites Under Tailored Sintering Cycles

**Zakaria Ahmad FARAG ALDALIMI[1],**
**Aboubaker Alferjani H. ALRAJHE[2],**
**Abdullatif Emar S ABO SBIA[3],**
**Mehmet AKKAŞ[4]**

## 1. INTRODUCTION

Powder metallurgy (PM) has emerged as a key manufacturing route for advanced composites when close control over chemical composition, particle level homogeneity, and microstructural architecture is required. In contrast to casting or deformation-based processing, PM offers efficient material utilization, enhanced microstructural uniformity, and near-net-shape capability benefits that are particularly relevant for components expected to perform under demanding tribological and corrosive conditions [1].

Cobalt containing systems are widely valued for their thermal stability, toughness, and chemical durability, which supports their use in aerospace, automotive, biomedical, precision mechanical, and energy-related applications [2]. Nevertheless, the practical performance of Co matrix composites is strongly governed by PM specific variables such as powder mixing quality, green density, diffusion-assisted bonding during sintering, and the resulting porosity network. In many PM composites, pore size and connectivity act as critical microstructural "defects" that can dominate both mechanical response and electrochemical degradation behavior [3,4].

[1] Department of Materials Science and Engineering, Graduate Education Institute, Kastamonu University, Turkey, zakariaaldalimi@outlook.com, ORCID: 0009-0003-2062-1218
[2] Department of Materials Science and Engineering, Graduate Education Institute, Kastamonu University, Turkey, aboubakeralferjani@outlook.com, ORCID: 0009-0003-6708-2178
[3] Department of Materials Science and Engineering, Graduate Education Institute, Kastamonu University, Turke, abdullatifemarsabosbia@outlook.com, ORCID: 0009-0002-5922-7878
[4] Assoc. Prof. Dr., Department of Mechanical Engineering/Faculty of Engineering, Architecture and Design, Kahramanmaraş İstiklal University, Kahramanmaraş, Turkey, mehmet.akkas@istiklal.edu.tr, ORCID: 0000-0002-0359-4743

In recent years, Co-matrix composite designs have gained momentum because they offer a pathway to tailor performance beyond monolithic alloys particularly by improving wear resistance, structural integrity, and corrosion tolerance through controlled microstructural engineering [5-8]. Despite this interest, a clear understanding is still needed regarding how changes in alloying/additive level influence densification behavior, pore evolution, and the coupled microstructure–property relationships in PM processed Co matrix composites [9-11].

Accordingly, this study examines the producibility of Co matrix composite structures manufactured via powder metallurgy, with emphasis on how composition-driven changes affect densification, pore morphology, microstructural features, and performance indicators including microhardness.

## 2. RESEARCH SIGNIFICANCE AND OBJECTIVES

The central aim of this work is to establish property microstructure linkages in cobalt matrix composites produced by PM by systematically evaluating how composition variation influences: Powder-stage homogeneity: mixing effectiveness and particle-level interactions, Densification behavior: green density consistency, sinter shrinkage tendency, and porosity distribution, Microstructural evolution: morphology and spatial distribution of phases as revealed by SEM and elemental mapping, Performance response: microhardness trends and corrosion-related electrochemical behavior. Key points highlighted by this study Co-matrix composites were manufactured successfully through a repeatable PM route. SEM observations indicate that porosity morphology and densification state are highly sensitive to composition level under fixed compaction and sintering conditions.

Overall, the findings offer practical guidance for optimizing composition and processing to obtain Co matrix composite systems with improved structural integrity and corrosion tolerance for industrially relevant applications.

## 3. MATERIALS AND METHODS

To investigate producibility and densification response, four powder batches were prepared from elemental powders (purity 99.9%, particle size 325 mesh). A cobalt matrix base formulation was selected, and the composition was varied by adjusting the level of the targeted constituent(s) to quantify its effect on microstructural development and electrochemical behavior. Powders were weighed using a precision balance and blended in a three-dimensional Turbula mixer for 5 hours to promote homogeneous distribution. This mixing strategy was chosen to minimize segregation and to support consistent green compact formation.

All powder mixtures were uniaxially compacted under a constant pressure of 625 MPa to produce green compacts with identical geometry. Sintering was performed in a controlled argon atmosphere at 585 °C for 3 minutes, aiming to limit oxidation while promoting diffusion bonding and interparticle neck growth. After sintering, samples were prepared by standard metallographic procedures (grinding, polishing, and etching). Microstructural assessment was carried out using SEM; selected areas were evaluated using elemental mapping to verify spatial distribution of phases/constituents. Microhardness measurements were performed along a defined line with 100 μm step size to capture local variations and to quantify heterogeneity typical of PM composites.

## 4. RESULTS AND DISCUSSION

SEM examinations reveal that the PM route enabled effective metallurgical bonding and generally uniform distribution of the cobalt matrix and associated constituent, reflecting adequate powder mixing and sintering effectiveness (Figures 1–3). The most pronounced microstructural differences among the four batches are associated with porosity morphology and pore connectivity, which are direct indicators of densification kinetics under the applied thermal cycle.

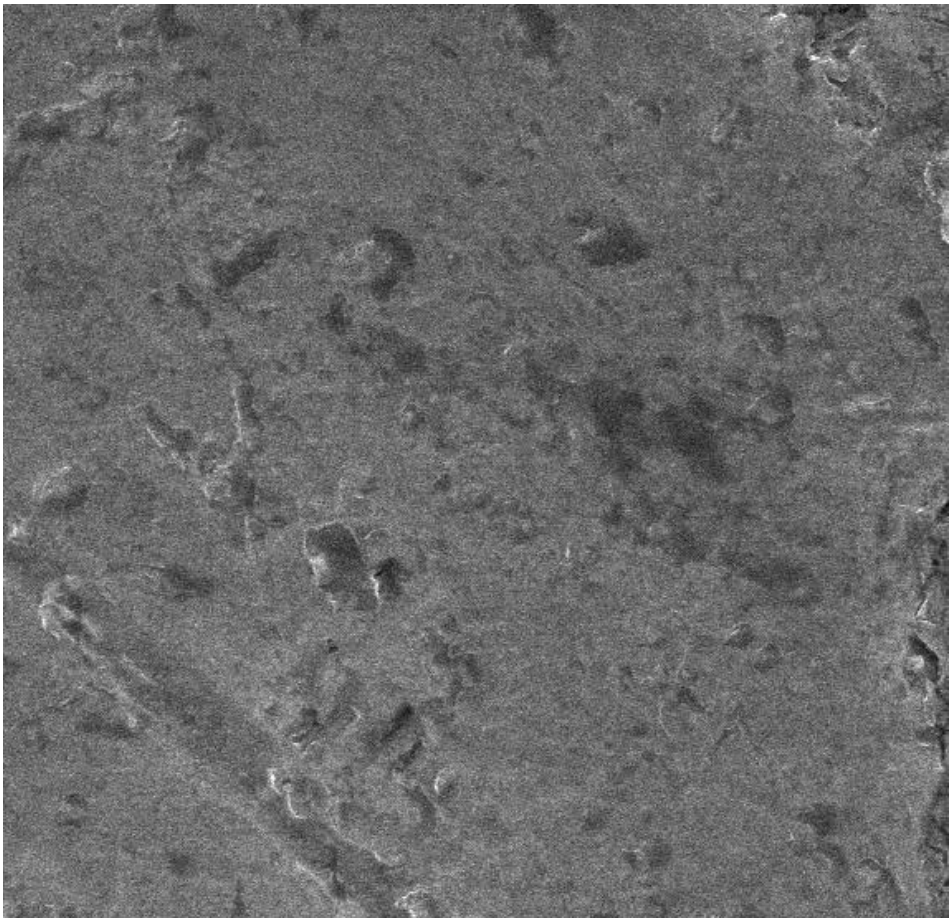

**Figure 1.** SEM Analysis image of sample number 1

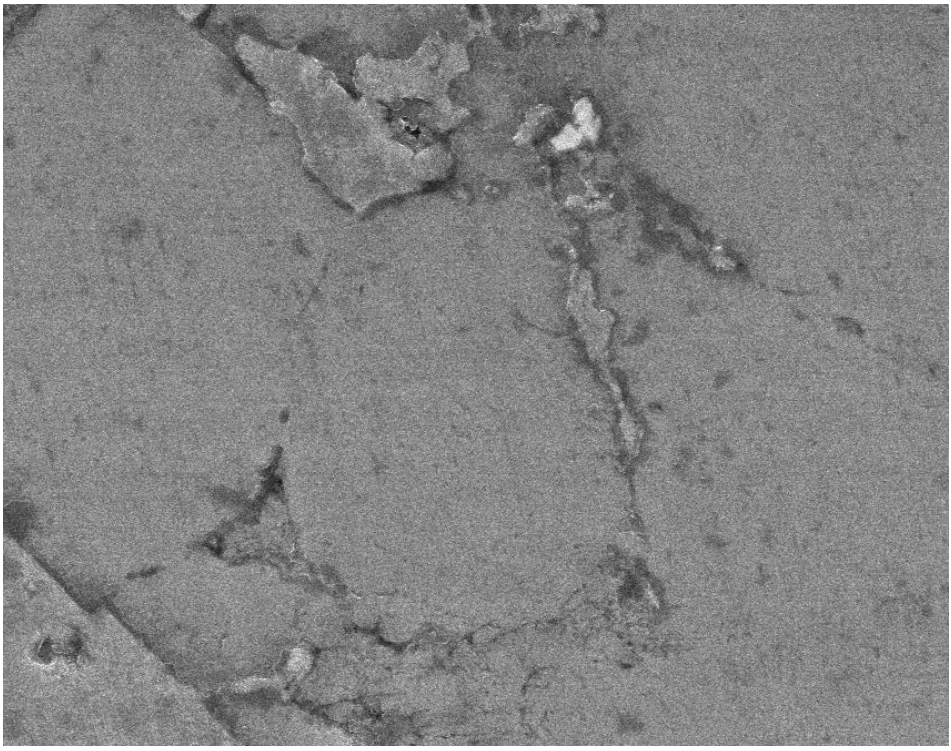

**Figure 2.** SEM Analysis image of sample number 2

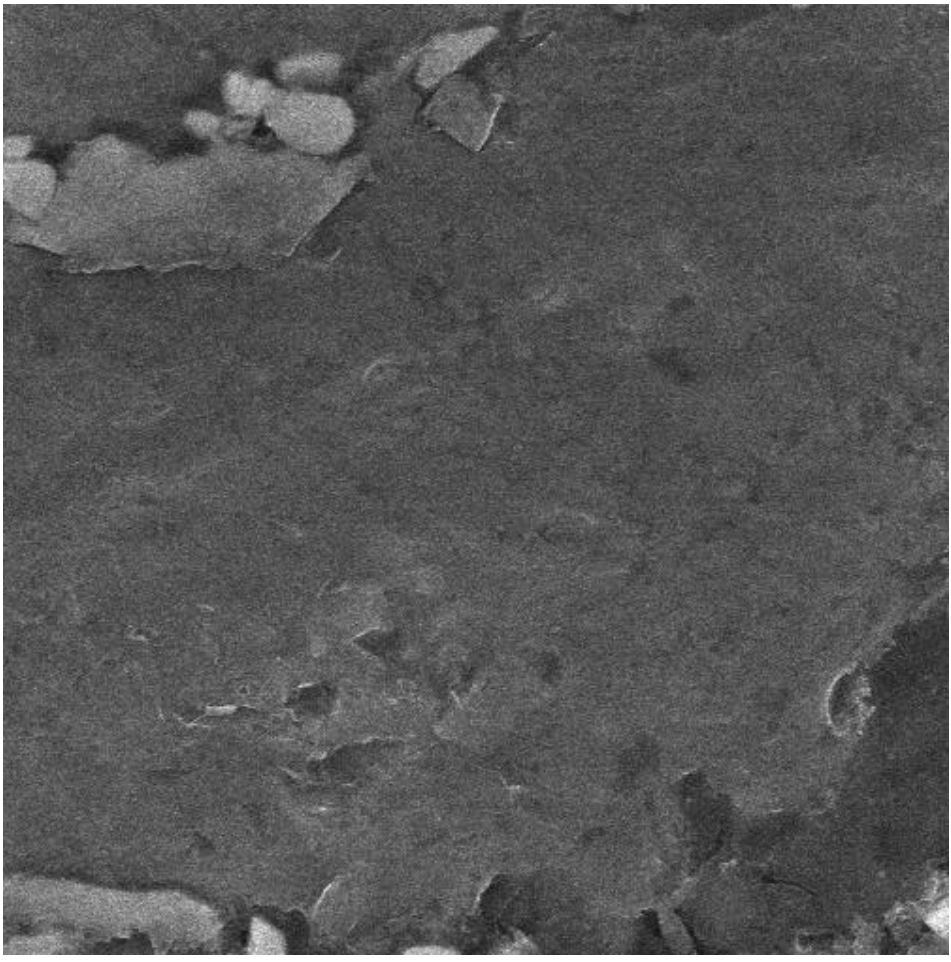

**Figure 3.** SEM Analysis image of sample number 3

With increasing composition level, pore size distribution and pore geometry showed measurable changes, consistent with composition-dependent diffusion activity and local sintering dynamics [12-15]. In some regions, localized voids and microcrack-like features were observed, suggesting incomplete densification or local constraint effects during sintering. These features are important because they can reduce load-bearing capacity and accelerate electrochemical penetration, thereby linking microstructure directly to performance outcomes. The observed trends support literature reports that diffusion-active elements and composition changes can alter neck growth rate, shrinkage behavior, and the final density state when sintering conditions are held constant [16,17]. In this context, the present results demonstrate that composition control is a primary lever for tuning densification response and structural integrity in Co-matrix PM composites.

Microhardness results obtained from line scanning at 100 μm intervals. The matrix-dominant sample exhibited an average hardness of approximately 111 HV, representing the baseline mechanical resistance of the cobalt matrix system. As the composition level was increased in subsequent batches, hardness rose to approximately 121 HV and then 124 HV, indicating that composition variation contributes to strengthening.

This increase can be attributed to a combination of reduced local deformation capacity due to microstructural refinement and/or phase redistribution, improved interparticle bonding associated with enhanced densification in optimized batches, and potential interface strengthening effects between the matrix and the compositionally modified regions created during sintering [18-20]. The highest hardness value recorded suggests that the selected upper-level composition in the current design space provides the most favorable strengthening contribution under the applied processing conditions [21-23].

Importantly, the line based hardness mapping highlights that PM composites can show spatial heterogeneity; therefore, interpreting hardness together with SEM-observed porosity and phase distribution provides a more reliable assessment than relying on a single-point measurement.

## 5. CONCLUSIONS

This study confirms that composition variation in powder metallurgy cobalt matrix composites strongly governs densification behavior and the resulting microstructure–property relationships. Under fixed compaction and sintering conditions, the following conclusions can be drawn: The PM route successfully produced Co matrix composites with repeatable geometry and analyzable microstructures. SEM analyses show that pore morphology, pore distribution, and densification state are highly sensitive to composition level, directly influencing structural integrity. Microhardness increased systematically across the tested composition range, reaching a maximum of 124 HV in the batch with the highest composition level.

## REFERENCES


1. Rominiyi, A. L., & Mashinini, P. M. (2023). Spark plasma sintering of discontinuously reinforced titanium matrix composites: densification, microstructure and mechanical properties—a review. The International Journal of Advanced Manufacturing Technology, 124(3), 709-736.
2. Praneeth, V. D., Manikandan, R., Pranav, A. S., Annamalai, A. R., & Muthuchamy, A. (2025). Influence of ball milling on the evolution of microstructure and microtexture in hot-press sintered cobalt alloy. Intermetallics, 176, 108548.
3. Barua, A., Pradhan, S., Priyadarshini, M., Patra, A., & Kumari, K. (2025). Recent advancement in tungsten heavy alloy processing for different industrial applications. Journal of Materials Engineering and Performance, 34(10), 8232-8252.
4. Juárez-López, F., Cuamatzi-Meléndez, R., Morales-Ramírez, Á. D. J., García-Hernández, M., & Carrera-Jota, M. L. (2024). Microstructural evolution and densification of Co-based alloy powder by spark plasma sintering for high-hardness applications. Coatings, 14(4), 479.
5. Patel, R., Karthik, G. M., & Sharma, P. (2025). Processing, Microstructure, and Mechanical Behavior of Tungsten Heavy Alloys for Kinetic Energy Penetrators: A Critical Review. Journal of Manufacturing and Materials Processing, 9(6), 186.
6. Oguntuyi, S. D., Johnson, O. T., & Shongwe, M. B. (2021). Spark plasma sintering of ceramic matrix composite of TiC: microstructure, densification, and mechanical properties: a review. The International Journal of Advanced Manufacturing Technology, 116(1), 69-82.
7. Wąsik, A., Madej, M., Rubach, R., Strojny-Nędza, A., Chmielewski, M., Garbiec, D., & Leszczyńska-Madej, B. (2026). Optimizing FAST/SPS parameters for ultra-high SiC content Al–SiC composites: thermal performance and microstructural insights. Archives of Civil and Mechanical Engineering, 26(2), 34.
8. Schramm Deschamps, I., dos Santos Avila, D., Vanzuita Piazera, E., Dudley Cruz, R. C., Aguilar, C., & Klein, A. N. (2022). Design of in situ metal matrix composites produced by powder metallurgy—a critical review. Metals, 12(12), 2073.
9. Buravlev, I. Y., Lembikov, A. O., Belov, A. A., Pisarev, S. M., Ponomareva, E. A., Kolodeznikov, E. S., ... & Papynov, E. K. (2025). Microstructure Evolution and Phase Formation in WC-TiC-TaC-HfC (-ZrC) High-Entropy Carbide Systems During Mechanical Activation and Spark Plasma Sintering. Journal of Composites Science, 9(12), 647.

**10.** Amos, Z. K. (2019). Spark plasma sintering of alumina reinforced with tungsten carbide-cobalt systems (Master's thesis, Botswana International University of Science and Technology (Botswana)).

**11.** Li, X. Y., Zhang, Z. H., Cheng, X. W., Huo, G. J., Zhang, S. Z., & Song, Q. (2021). The development and application of spark plasma sintering technique in advanced metal structure materials: A review. Powder Metallurgy and Metal Ceramics, 60(7), 410-438.

**12.** Lores, A., Azurmendi, N., Agote, I., & Zuza, E. (2019). A review on recent developments in binder jetting metal additive manufacturing: materials and process characteristics. Powder Metallurgy, 62(5), 267-296.

**13.** Aljabr, R. Y., & Bose, P. S. C. (2025). Fabrication and Characterization of Mg-HAP Nanocomposites via Powder Metallurgy. Journal of Materials Engineering and Performance, 1-14.

**14.** Fazili, A., Nikzad, L., & Razavi, M. (2025). Optimization of mechanical properties in hybrid (TiCN-WC)/Co cermets prepared via spark plasma sintering. International Journal of Refractory Metals and Hard Materials, 107642.

**15.** Ali, A., Park, K. R., Song, Y., Jeong, D. W., Haq, M. A., & Kim, B. S. (2025). In-situ TiN formation and microstructural evolution in WC–Co–Ti composites via gas-phase nitridation and spark plasma sintering. International Journal of Refractory Metals and Hard Materials, 107638.

**16.** Zhang, X., Zhou, Y., Wan, H., Xu, G., Xu, W., Zhu, Y., & Lei, Q. (2025). Effect of TiC content on the microstructure and properties of Cu matrix composites with enhanced softening and wear resistance. Materials Characterization, 115798.

**17.** Wang, Z., Zhu, X., Wang, C., Xiao, X., Zhang, K., Jiang, C., & Liu, J. (2025). Microstructure and mechanical properties of Al/Cu-SS hybrid composite via ball milling and friction stir processing. iScience, 28(12).

**18.** Zhang, M., Ma, D., Wang, J., Dai, S., Xue, Y., & Zhu, L. (2025). Enhancing interfacial bonding in metal matrix composites: challenges, methods, and future prospects. Critical Reviews in Solid State and Materials Sciences, 1-54.

**19.** Pooja, K., Tarannum, N., & Chaudhary, P. (2025). Metal matrix composites: revolutionary materials for shaping the future. Discover Materials, 5(1), 35.

**20.** Li, R., Wang, X., Li, J., & Jia, P. (2025). Research progress on reinforcing particles, preparation process, heat treatment, and hot deformation of particle-reinforced stainless steel matrix composites. Journal of Materials Science, 1-35.

**21.** Das, P., Pathak, D. K., Sharma, P., & Pandey, P. M. (2025). A review on the mechanical and biocorrosion behaviour of iron and zinc-based biodegradable materials fabricated using powder metallurgy routes. Corrosion Reviews, 43(3), 279-300.

**22.** Bendjemil, B., AjiliI, L., Safi, K., Sassi, S., Ferhi, M., & Naifer, K. H. (2025). Tailoring the Mechanical and Microstructural Properties of Ti-Zr-Based Carbide Composites via Spark Plasma Sintering: Impact of Molybdenum and Tungsten Additions.

**23.** Wen, M., Jiang, B., Duan, X., & Xiang, D. (2025). Research Progress on Microstructure, Mechanical Properties, and Strengthening Mechanisms of In Situ-Synthesized Ceramic-Reinforced Titanium Matrix Composite Coatings via Laser Cladding. Coatings, 15(7), 815.